No. 2026-009

When Openings Change Future Openings:
A Fast–Slow Model of Experience-Dependent Transition Laws in Self-Referential Cognition

September 2, 2026

Takanori Suzuki

When Openings Change Future Openings:

A Fast–Slow Model of Experience-Dependent Transition Laws in Self-Referential Cognition

Takanori Suzuki[1]

September 2, 2026

Research Institute of Business Administration (Sanken), Waseda University
Working Paper Series, No. 2026-009

Working paper note. This paper is the fourth in a research program on mental quieting, self-referential psychological memory, entry into attention, and experience-dependent learning. The preceding papers are RIBA Working Paper No. 2026-006 (*Two Dynamics toward Mental Quieting: A Comparative Model of Faith-Mediated and Self-Observation Pathways*), No. 2026-007 (*When Memory Governs Memory: An Endogenous-Operator Model of Recursive Psychological Activity*), and No. 2026-008 (*The Dynamics of Entry into Attention: A Point Process of Candidate Openings toward Functional Non-Closure*). A journal-submission version of the present paper was submitted to the *Journal of Mathematical Psychology* on September 2, 2026. The journal submission and this working paper share the same core model, analytical results, and numerical illustrations; the present working paper consolidates the main text and its technical appendix in a single document. A reproduction script, machine-readable numerical outputs, and vector figures accompany this paper.

Abstract

Repeated openings in self-referential cognition need not leave later episodes governed by the same transition law. I develop a fast–slow model with a cross-episode state, operator legibility ℓ_n, defined as the ease with which recurrent self-referential operator structure becomes recognizable when it reappears. Within an episode, ℓ_n changes the efficiency of structural-visibility formation in a fast system of curiosity, visibility, acquisition–achievement pressure, and object sensitivity. Across episodes, qualified experience raises ℓ_n, while natural loss and evaluative capture lower it. A three-state layer distinguishes unresolved self-referential activation, entry into functional non-closure with preserved object sensitivity, and fusion, with re-closure after entry. Higher legibility orders the later transition kernel: attention-entry intensity rises, competing fusion falls, and first re-closure is delayed under matched conditions. The same slow state lowers the post-withdrawal watershed; above a critical $\ell^\dagger$, a positive persistence basin exists and expands. Because the slow map also admits flat and reverse-learning regions, repetition is not assumed to help. Numerical examples illustrate transition improvement, learning-induced birth of persistence, and reversal under evaluative capture. Closing the loop—generating qualified experience from the stochastic episode process itself—produces path-dependent learning: identically parameterized replications diverge in whether and when they cross the persistence threshold, and the constant-summary benchmark can overstate what the loop endogenously sustains. The model therefore

[1]Faculty of Commerce, Waseda University. Email: suzuki@waseda.jp. ORCID: 0009-0008-8955-7003.

treats learning as an experience-dependent change in future transition law, not as accumulated attention or a stronger observing agent.

Keywords: experience-dependent transition; operator legibility; fast–slow dynamics; competing risks; self-referential cognition; bistability.
JEL classification: C41; C61; D83; D91; I12.

1 Introduction

A recurrent self-referential movement need not unfold in the same way each time it reappears. In one episode it may remain opaque for a long interval; in a later, structurally similar episode it may become visible sooner. Fusion may become less likely, and re-closure after entry may become less frequent. These differences raise a question that is distinct from whether the current state has improved: *can an earlier opening change the law governing a later transition?*

The distinction is between current visibility and future recognizability. Let $v_n(t)$ denote how visible recurrent memory dynamics are within episode n, and let $\ell_n \in [0, 1]$ denote *operator legibility*: how readily recurrent self-referential operator structure becomes recognizable when it reappears. A high $v_n(t)$ is a present state; a high ℓ_n is a history-dependent condition on the next episode. The immediate predecessor allows repeated opening episodes, but conditional on the fast state path and fixed parameters, its event process carries no learning from prior openings into the next episode (Suzuki, 2026). The present paper endogenizes that missing cross-episode state.

The model has two time scales. Within episode n, the fast state is

$$X_n(t) = (q_n(t), v_n(t), g_n(t), \kappa_n(t)), \tag{1.1}$$

where q is object-centered curiosity, v current structural visibility, g acquisition–achievement pressure, and κ object sensitivity. Operator legibility is fixed within an episode and changes visibility formation through

$$a_v(\ell) = a_{v0} + a_{v1}\ell, \qquad a_{v1} \geq 0. \tag{1.2}$$

Across episodes,

$$\ell_{n+1} = \ell_n + \eta Y_n(1 - \ell_n) - \{\delta_\ell + \chi G_n\}\ell_n, \tag{1.3}$$

where Y_n is qualified experience and G_n episode-level evaluative capture. Thus experience can form legibility, while natural loss and the conversion of observation into an achievement project can erode it. A three-state layer distinguishes unresolved self-referential activation R, functional non-closure with preserved object sensitivity A, and fusion F,

$$R \xrightarrow{\lambda_A(t;\ell)} A, \qquad R \xrightarrow{\nu_F(t;\ell)} F, \qquad A \xrightarrow{\mu_R(t;\ell)} R. \tag{1.4}$$

The slow state is therefore not an attention stock or a stronger observing agent. It changes the efficiency with which recurrent structure becomes visible, after which the inherited fast dynamics propagate that change.

Two results organize the paper. First, under matched inputs and initial fast states, higher legibility raises the attention-entry intensity and lowers the competing fusion and matched-state re-closure intensities. The cause-specific attention clock is stochastically earlier, fusion has lower cumulative incidence, and first re-closure is delayed. Second, the same slow state changes post-withdrawal geometry. Under a constant episode environment,

$$\ell^* = \frac{\eta\bar{Y}}{\eta\bar{Y} + \delta_\ell + \chi\bar{G}} \tag{1.5}$$

is the stationary legibility target. When the visibility-formation threshold is interior, a critical level $\ell^\dagger$ separates a region with no positive saddle–attractor pair from a region with a positive persistence basin. For $\ell > \ell^\dagger$, the saddle watershed moves inward and the positive basin expands. Hence $\ell^* > \ell^\dagger$ permits a finite learning-induced crossing into persistence geometry, whereas $\ell^* \leq \ell^\dagger$ permits transition improvement without self-sustaining post-withdrawal geometry. If the current ℓ lies above its slow target, the same model generates reverse learning.

Because qualified experience is itself an output of the stochastic episode process, closing the loop makes the slow path random: identical parameters and initial conditions can produce divergent learning histories, the crossing into persistence geometry becomes an event with a dispersed arrival episode rather than a deterministic date, and the constant-summary benchmark can be endogenously unattainable (Section 8).

The contribution is deliberately narrow. Learning, perceptual discrimination, decentering, recurrent-event models, and critical transitions provide close neighboring ideas (Goldstone, 1998; Watanabe and Sasaki, 2015; Bernstein et al., 2015; Andersen and Gill, 1982; Scheffer et al., 2009). This paper does not replace those accounts. It links a slow state of recurrent-operator legibility to a fast transition system and shows that one experience-dependent state can order both later entry/fusion/re-closure and the deterministic geometry of post-withdrawal persistence. The model therefore treats learning as a change in future transition law rather than as accumulated attention. It also preserves negative regions: repetition can be beneficial, neutral, or counterproductive depending on qualified experience, natural loss, and evaluative capture. The paper makes no therapeutic-efficacy or economic-optimality claim; those require empirical identification and a separate value problem.

2 Related Work and Positioning

The model sits at the intersection of four literatures, but its contribution is narrower than any claim to replace them. First, work on habituation and habit formation establishes that repetition can change later responding and that such change can be history dependent (Groves and Thompson, 1970; Lally et al., 2010; Wood and Rünger, 2016; Watkins and Nolen-Hoeksema, 2014). The learned object in the present paper is different: it is not automatic execution of a response but the ease with which a recurrent operator structure becomes discriminable. In that sense the closest analogy is perceptual learning, which studies experience-dependent improvements in extracting or discriminating structure from sensory input (Goldstone, 1998; Watanabe and Sasaki, 2015). The present model adds a dynamical consequence to that analogy: improved legibility changes later transition intensities and can change the geometry of persistence after external support is removed.

Second, decentering, cognitive defusion, meta-awareness, and related contemplative constructs describe changes in the relation to ongoing thought rather than simple removal of thought content (Bernstein et al., 2015; Gillanders et al., 2014; Bolderston et al., 2019; Lutz et al., 2015; Schooler et al., 2011). These constructs motivate the distinction between a self-referential activation state and entry into functional non-closure, but they do not supply the slow cross-episode state used here. Computational accounts of meta-awareness and attentional-state shifts likewise formalize within-episode regulation or autonomous switching (Sandved-Smith et al., 2021; Oyama et al., 2025; Laukkonen and Slagter, 2021). The present paper instead asks how a prior qualified episode changes the law of the next episode.

Third, recurrent-event, competing-risk, and multi-state methods provide a natural language for transition intensities and first-event comparisons (Andersen and Gill, 1982; Hougaard, 1999; Putter et al., 2007). These methods are used as mathematical tools rather than presented as methodological innovations. The substantive object is the endogenous ordering of three transitions—entry, fusion, and re-closure—generated by a common slow state through the fast dynamics.

Fourth, bistability and critical-transition research shows how qualitatively different long-run states can coexist and how parameter changes can move a system across a tipping point (Scheffer et al., 2009; van de Leemput et al., 2014; Cramer et al., 2016; Haslbeck et al., 2022). The present model does not claim novelty for bistability itself. Its geometric contribution is to make the relevant bifurcation parameter an experience-dependent state. Operator legibility changes the visibility-formation coefficient, thereby moving the saddle watershed and, in a near-critical region, creating the saddle–attractor pair itself.

The narrow theoretical gap is therefore this: existing neighboring literatures separately provide repetition-dependent change, altered relations to thought, multi-state transition tools, and critical-transition geometry. The present model combines these elements in an experience-dependent transition architecture in which qualified openings can change operator legibility, and that slow change jointly alters later entry, fusion, re-closure, and post-withdrawal persistence.

3 Model

3.1 Baseline construct and the new margin

The paper uses a reduced-form construct of self-referential cognition. Memory-generated operations may interpret, correct, justify, punish, or monitor present experience; *functional closure* denotes the extent to which those outputs are re-entered as if they were present facts. A model-level opening toward *functional non-closure* therefore means weaker re-entry, and an attention entry additionally requires preserved sensitivity to the present object. These are theoretical state definitions, not clinical diagnoses or claims about the ontology of attention.[2]

A running vignette. A concrete episode may help fix the constructs before they are formalized. Suppose a recurrent self-critical movement re-enters during work: an inner commentary corrects, ranks, and judges the present performance. While its output is simply lived as fact ("this is going badly"), the operator is enacted but not seen. The moment the movement becomes conspicuous *as a recurring structure* ("this is the same commenting pattern again"), current visibility v is high. Whether that moment arrives easily in the *next* structurally similar episode is a different quantity;

[2]Throughout, "attention entry" and the state label A are technical terms for the transition into functional non-closure with preserved object sensitivity (Definition 3.5); they are not used in the sense of selective attention, attentional resource allocation, or vigilance in the experimental attention literature, and no claim about those constructs is intended.

that ease is operator legibility ℓ. Wanting to watch the pattern more closely because it is interesting is curiosity q; continuing to register what the present task is actually doing is object sensitivity κ. If observing the pattern itself becomes a project to succeed at—being a good observer, securing a quiet mind, hitting an attention KPI—acquisition–achievement pressure g rises, and the episode-level summary of that pressure is evaluative capture G. The three discrete outcomes introduced below correspond to the movement remaining unresolved (R), the commentary being watched as structure while task contact is preserved (A), and the commentary being lived as fact with the object lost (F). The vignette is illustrative only; the model is stated over the abstract states.

The immediate predecessor endogenized a state-dependent opening intensity using curiosity q, current structural visibility v, acquisition–achievement pressure g, and object sensitivity κ (Suzuki, 2026). Conditional on those state paths and fixed individual parameters, however, earlier opening events did not change the next episode's transition law. The present paper is self-contained and restates the fast system below. Its new elements are: a cross-episode state ℓ, a fast-to-slow experience bridge, a competing fusion transition, and post-entry re-closure. Only one inherited coefficient becomes learning sensitive, $a_v(\ell)$, so the extension can be evaluated without changing the rest of the fast architecture.

3.2 Episodes and two time scales

Let episodes be indexed by $n = 0, 1, 2, \ldots$. Within episode n, continuous time is denoted by $t \in [0, T_n]$. The slow state ℓ_n is fixed over that interval and may change only at the boundary between episodes. The within-episode continuous state is

$$X_n(t) := \big(q_n(t), v_n(t), g_n(t), \kappa_n(t)\big), \tag{3.1}$$

with state space

$$\mathcal{X} = [0,1] \times [0,1] \times \mathbb{R}_+ \times [0,1]. \tag{3.2}$$

The episode-level slow state satisfies

$$\ell_n \in [0,1]. \tag{3.3}$$

The model therefore has two clocks: a fast clock t describing the unfolding of a particular self-referential episode, and a slow clock n describing how the conditions of recognition may change across episodes; the fast–slow terminology follows the general theory of multiple-time-scale dynamics (Kuehn, 2015).

The separation is substantive, not only technical. The fast variable $v_n(t)$ answers the question "how visible is the structure now?" The slow variable ℓ_n answers the different question "if a comparable operator pattern appears again, how readily can that pattern become visible?" The model will never identify these two quantities.

Definition 3.1 (Current visibility). $v_n(t) \in [0,1]$ *is the within-episode visibility of memory dynamics: the degree to which repetition, contradiction, stereotypy, and operator-on-operator structure are currently visible as structure rather than only enacted as content.*

Definition 3.2 (Operator legibility). $\ell_n \in [0,1]$ *is the episode-level* operator legibility*: the ease with which a recurrent self-referential operator pattern can become structurally* *recognizable when it appears in episode n. It is a slow condition on recognition, not the amount of attention accumulated in the past and not the strength of an observing agent.*

The same remembered content may therefore occur with different pairs (v, ℓ). A person may have high long-run legibility but low current visibility because the present episode is unusually intense or because acquisition–achievement pressure is high. Conversely, a particular episode may momentarily make a pattern highly visible even when little of that visibility carries forward. This distinction is necessary if the model is to represent learning without collapsing learning into the current attention state.

3.3 Inherited fast subsystem

External token intensity is $u_n(t) \geq 0$, and $z_n(t) \geq 0$ denotes direct evaluation or reward tied to the inner outcome itself (an attention KPI). Task contact is represented by the increasing, concave function

$$\mathcal{E}(u) = 1 - e^{-\alpha u}, \qquad \alpha > 0. \tag{3.4}$$

Conditional on ℓ_n, the fast states evolve as

$$\dot{q}_n = a_q \mathcal{E}(u_n)(1 - q_n) + \rho v_n q_n (1 - q_n) - \{d_q + b_q g_n\} q_n, \tag{3.5}$$

$$\dot{v}_n = a_v(\ell_n) q_n (1 - v_n) - d_v v_n, \tag{3.6}$$

$$\dot{g}_n = a_g u_n + a_z z_n - d_g g_n, \tag{3.7}$$

$$\dot{\kappa}_n = a_\kappa q_n v_n (1 - \kappa_n) - \{d_\kappa + b_\kappa g_n\} \kappa_n. \tag{3.8}$$

All primitive coefficients in (3.5)–(3.8) are positive unless explicitly allowed to be zero below. The baseline learning-sensitive visibility coefficient is

$$a_v(\ell) = a_{v0} + a_{v1}\ell, \qquad a_{v0} > 0, \quad a_{v1} \geq 0. \tag{3.9}$$

Thus ℓ does not directly manufacture an opening. Its primary structural role is to change how efficiently object-centered curiosity is converted into the current visibility of memory dynamics.

The interpretation of the four fast states is unchanged. q is object-centered curiosity, the degree to which engagement is driven by wanting to see more of the object rather than by reward acquisition. v is current structural visibility. g is acquisition–achievement pressure, including pressure generated by reward, success, self-evaluation, or “correct observation.” κ is object sensitivity, the degree to which new information from the present object continues to enter the response. In particular, low self-referential activity without preserved κ is not treated as attention; withdrawal and dissociation must remain conceptually separate from functional non-closure.

Assumption 3.3 (Within-episode inputs and state domain)**.** *For each episode, u_n and z_n are bounded, nonnegative, piecewise-continuous functions. Initial conditions satisfy $q_n(0), v_n(0), \kappa_n(0) \in [0, 1]$ and $g_n(0) \geq 0$. The slow state ℓ_n is fixed during the episode.*

Under Assumption 3.3, the right-hand side of (3.5)–(3.8) is locally Lipschitz. Boundary signs also point inward on $q, v, \kappa \in [0, 1]$, while g cannot cross below zero. Hence the fast system is well posed on the intended state domain. The later analytical sections will use this invariance rather than re-derive the state ontology.

The baseline keeps d_v fixed. A secondary robustness specification may allow persistence itself to depend on legibility,

$$d_v(\ell) = d_{v0}e^{-\omega_v \ell}, \qquad \omega_v \geq 0, \tag{3.10}$$

but no central theorem will require this additional channel. Likewise, a direct term $\theta_\ell \ell$ in the entry intensity is reserved for robustness analysis. The main model forces the effect of ℓ on entry to pass first through the observable fast dynamics, especially v.

3.4 From candidate openings to model-level attention entry

Conditional on the fast path, candidate openings toward functional non-closure arrive with intensity

$$\lambda_O(t; \ell_n) = \lambda_0 \exp\{\theta_q q_n(t) + \theta_v v_n(t) + \theta_\kappa \kappa_n(t) - \theta_g g_n(t)\}, \tag{3.11}$$

where $\lambda_0, \theta_q, \theta_v, \theta_\kappa, \theta_g > 0$. A candidate opening is not yet a model-level attention entry. Let $\pi : [0,1] \to [0,1]$ be nondecreasing. The attention-entry intensity is the object-sensitivity-thinned intensity

$$\lambda_A(t; \ell_n) = \lambda_O(t; \ell_n)\, \pi(\kappa_n(t)). \tag{3.12}$$

Equation (3.12) preserves the preceding paper's distinction between an opening opportunity and an entry that remains responsive to the present object. The new slow state does not change that ontology.

The absence of a direct ℓ term from (3.12) is intentional. If a larger ℓ simply appeared as $+\theta_\ell \ell$ in the exponent, the statement "greater legibility raises entry" would be partly built into the hazard by definition. In the baseline model, the stronger claim must instead come from the coupled path: greater ℓ raises $a_v(\ell)$, which can raise v, which can feed q and κ, and only then raise λ_A. This leaves the entry result to be proved rather than assumed.

3.5 Three-state transition architecture

The point-process entry model is extended by distinguishing three episode-local discrete states,

$$S_n(t) \in \{R, A, F\}. \tag{3.13}$$

They are defined as follows.

Definition 3.4 (Self-referential activation state R)**.** *R is the state in which self-referential psychological activity is operative and the episode has not yet resolved into either model-level attention entry or fusion. R is not a pathology label; it is the baseline unresolved state from which the competing transitions are evaluated.*

Definition 3.5 (Attention-entry state A)**.** *A is an episode-local state of functional non-closure with preserved object sensitivity. Entry into A occurs at intensity λ_A in* (3.12)*. The state does not imply permanent quieting, and it is not absorbing: self-referential closure can recover.*

Definition 3.6 (Fusion state F)**.** *F is the episode-local state in which self-referential processing has become dominant before attention entry, so that operator output is* *effectively enacted as present fact and object sensitivity is substantially lost. F is absorbing only within the baseline episode. It is not a diagnosis and does not imply permanent fusion across future episodes.*

The baseline transition graph is

$$R \xrightarrow{\lambda_A(t;\ell_n)} A, \qquad R \xrightarrow{\nu_F(t;\ell_n)} F, \qquad A \xrightarrow{\mu_R(t;\ell_n)} R. \tag{3.14}$$

A direct $A \to F$ edge is omitted in the baseline. If an A episode closes again, it first returns to R, after which entry and fusion again compete under the current fast state. This makes re-closure conceptually distinct from immediate fusion and keeps the competing-risk interpretation transparent. A direct $A \to F$ channel can be added as a robustness extension without altering the role of ℓ.

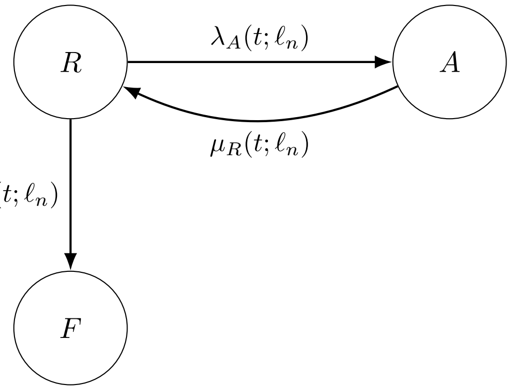

Figure 1: Episode-local transition architecture. Entry and fusion compete from R; A may re-close to R; F is absorbing only for the current episode.

The specific hazard forms are fixed at this stage even though their comparative statics are postponed. The baseline fusion hazard is

$$\nu_F(t;\ell_n) = \nu_0 \exp\{\phi_g g_n(t) - \phi_v v_n(t) - \phi_\kappa \kappa_n(t)\}, \tag{3.15}$$

and the re-closure hazard is

$$\mu_R(t;\ell_n) = \mu_0 \exp\{\psi_g g_n(t) - \psi_v v_n(t) - \psi_\kappa \kappa_n(t)\}. \tag{3.16}$$

Here $\nu_0, \mu_0 > 0$, $\phi_g, \psi_g > 0$, and the coefficients on v and κ are nonnegative (strictly positive in the baseline interpretation). Equations (3.15)–(3.16) are reduced-form transition laws, not definitions of attention. Curiosity does not enter (3.15) directly: in the baseline, wanting to see more of the object is neither protective against nor conducive to fusion except through what it renders visible (v) and the sensitivity it sustains (κ); adding a protective $-\phi_q q$ loading would only strengthen the orderings established below. Importantly, ℓ has no direct loading in either central hazard. Its influence must first change the observable fast path through $a_v(\ell)$ and hence v and κ. Optional direct legibility loadings are treated only as robustness extensions in the Technical Appendix.

Conditional on ℓ_n, the input paths, and initial conditions, the continuous state $X_n(t)$ and discrete state $S_n(t)$ form a piecewise-deterministic within-episode system in the sense of Davis (1984). Across episodes, however, the process need not be stationary because ℓ_n is updated from experience. This is the precise sense in which the present paper moves from a state-dependent opening process to an experience-dependent transition law.

3.6 What the slow state learns

The slow state is updated only between episodes. Let $Y_n \in [0,1]$ denote a qualified-experience summary and let $G_n \in [0,1]$ denote an episode-level summary of acquisition–evaluation pressure. The next section will specify and solve the learning map

$$\ell_{n+1} = \mathcal{L}(\ell_n, Y_n, G_n). \tag{3.17}$$

At the constitutional stage, only the roles of Y_n and G_n are fixed.

A qualified experience is not simply "an A event occurred." It must preserve the distinction between inward absorption and functional non-closure. The fast episode therefore generates the two summaries that feed the slow update:

Definition 3.7 (Fast-to-slow episode summaries)**.** *Let*

$$\boxed{Y_n = \mathcal{Y}[S_n(\cdot), v_n(\cdot), \kappa_n(\cdot)] \in [0,1],} \tag{3.18}$$

and

$$\boxed{G_n = \mathcal{G}[g_n(\cdot), z_n(\cdot)] \in [0,1].} \tag{3.19}$$

The functional $\mathcal{Y}$ is nondecreasing in qualified exposure to A, current structural visibility, and preserved object sensitivity. It summarizes the experience-side formation opportunity only; the evaluative penalty is not subtracted again inside Y_n. The functional $\mathcal{G}$ summarizes the episode's acquisition–evaluation pressure path and carries that opposing channel separately.

No particular functional form is required for the analytical results below. One bounded canonical closure, useful for interpretation, is

$$Y_n = 1 - \exp\left\{ -\omega_Y \int_0^{T_n} \mathbf{1}_{\{S_n(t)=A\}} v_n(t)\kappa_n(t)\,dt \right\}, \tag{3.20}$$

$$G_n = 1 - \exp\left\{ -\omega_G \int_0^{T_n} g_n(t)\,dt \right\}, \tag{3.21}$$

with $\omega_Y, \omega_G > 0$. The central theorems condition on the realized summary sequence and therefore do not depend on this illustration. The constant-summary analysis later in the paper should be read as a benchmark for comparable repeated episodes, not as an assertion that the fully endogenous stochastic summaries are literally constant.

This is also where the term "learning" receives its restricted meaning. What changes is the future legibility of recurrent operator structure. The model does not say that attention is stored, that an observer acquires a new power, or that practice mechanically produces attention. A later opening remains an event whose occurrence is not guaranteed. Experience changes the conditions of transition; it does not abolish uncertainty in the transition itself.

Remark 3.8 (Relation to memory records)**.** *The slow scalar ℓ_n is not identical to either the rule-forming history or the non-recursive record introduced in the endogenous-operator model. It is a reduced-form coarse-graining of one possible consequence of prior* *experience: the ease with which recurrent operator structure can become recognizable. Keeping ℓ distinct from a full memory stock prevents the present paper from reopening the entire endogenous-operator architecture.*

Nestedness and scope. Freezing ℓ removes experience dependence; setting $a_{v1} = 0$ removes the legibility-to-visibility channel; and suppressing the added fusion and re-closure hazards recovers the inherited entry model. The model therefore isolates a single new margin: whether qualified experience changes the conditions of later recognition. It does not optimize interventions or assign welfare values.

4 Slow Learning Across Episodes

Complete proofs and auxiliary comparative statics are reported in the Technical Appendix.

The fast episode produces two bounded summaries: qualified experience $Y_n \in [0,1]$ and evaluative capture $G_n \in [0,1]$ (Definition 3.7). Operator legibility changes only between episodes according to

$$\ell_{n+1} = \ell_n + \eta Y_n(1 - \ell_n) - \{\delta_\ell + \chi G_n\}\ell_n, \tag{4.1}$$

where $\eta \geq 0$ is formation efficiency, $\delta_\ell \geq 0$ is natural loss, and $\chi \geq 0$ is sensitivity to evaluative capture. The formation term saturates as $\ell_n \to 1$; the loss term allows repeated experience to be neutral or counterproductive. To avoid discrete-time overshooting in the central specification, assume that every admissible episode satisfies

$$\eta Y_n + \delta_\ell + \chi G_n \leq 1. \tag{4.2}$$

Because $Y_n, G_n \in [0,1]$, the primitive bound $\eta + \delta_\ell + \chi \leq 1$ is sufficient for (4.2) but stronger than necessary; it is not imposed in the numerical illustrations, all of which satisfy (4.2) episode by episode (Section 8). Either way, (4.2) is a step-size convention rather than a substantive requirement; continuous-time and weaker discrete-time versions are in the Technical Appendix.

For the benchmark of comparable repeated episodes, set $Y_n \equiv \bar{Y}$ and $G_n \equiv \bar{G}$, and define

$$a := \eta\bar{Y}, \qquad b := \delta_\ell + \chi\bar{G}, \qquad r_\ell := 1 - a - b. \tag{4.3}$$

When $a + b > 0$, the stationary target is

$$\boxed{\ell^* = \frac{\eta\bar{Y}}{\eta\bar{Y} + \delta_\ell + \chi\bar{G}}}. \tag{4.4}$$

Theorem 4.1 (Slow-state convergence and learning direction)**.** *Under* (4.2)*, if* $a+b > 0$ *then*

$$\ell_n = \ell^* + r_\ell^n(\ell_0 - \ell^*), \qquad 0 \leq r_\ell < 1. \tag{4.5}$$

Hence ℓ_n *rises monotonically when* $\ell_0 < \ell^*$*, is constant when* $\ell_0 = \ell^*$*, and falls monotonically when* $\ell_0 > \ell^*$*. If* $a = b = 0$*, every* ℓ *is a fixed point.*

Equivalently, at a current value ℓ,

$$\ell_{n+1} - \ell_n = \eta\bar{Y}(1 - \ell) - (\delta_\ell + \chi\bar{G})\ell, \tag{4.6}$$

so positive, flat, and reverse learning correspond exactly to $\ell < \ell^*$, $\ell = \ell^*$, and $\ell > \ell^*$. This is the model's main safeguard against treating repetition as improvement by definition.

The same balance determines whether any target $h \in (0,1)$ can be sustained:

Proposition 4.2 (Target-feasibility condition)**.** *For $a + b > 0$,*

$$\ell^* > h \iff \eta\bar{Y}(1-h) > (\delta_\ell + \chi\bar{G})h. \tag{4.7}$$

Thus more episodes cannot carry the slow state beyond a threshold that lies at or above its stationary target.

The constant-summary case is a structural benchmark, not a claim that the fully endogenous functionals $\mathcal{Y}$ and $\mathcal{G}$ are literally constant. Nonstationary solutions and pathwise environment comparisons are given in the Technical Appendix.

5 Learning-Induced Persistence Geometry

Full equilibrium classification, branch comparative statics, and proofs are in the Technical Appendix.

After external inputs have been withdrawn and residual acquisition–achievement pressure has decayed, the inherited curiosity–visibility subsystem is

$$\dot{q} = q\{\rho v(1-q) - d_q\}, \tag{5.1}$$

$$\dot{v} = a(\ell)q(1-v) - d_v v, \qquad a(\ell) = a_{v0} + a_{v1}\ell, \tag{5.2}$$

with $\rho > d_q > 0$, $d_v > 0$, $a_{v0} > 0$, and $a_{v1} \geq 0$. This section asks only whether a self-sustaining post-withdrawal basin is geometrically available; it does not assert that an attention entry has occurred or that the realized state lies in that basin.

For a positive equilibrium, the two nullclines imply

$$\rho a q^2 - a(\rho - d_q)q + d_q d_v = 0, \tag{5.3}$$

with discriminant

$$\Delta_h(a) = (\rho - d_q)^2 - \frac{4\rho d_q d_v}{a}. \tag{5.4}$$

Hence the critical visibility-formation coefficient is

$$\boxed{a_v^* = \frac{4\rho d_q d_v}{(\rho - d_q)^2}}. \tag{5.5}$$

If $a < a_v^*$ there is no positive equilibrium; at equality a saddle–node fold occurs; and if $a > a_v^*$ there are two positive equilibria

$$q_\pm(a) = \frac{(\rho - d_q) \pm \sqrt{\Delta_h(a)}}{2\rho}, \qquad v_\pm(a) = \frac{a q_\pm(a)}{d_v + a q_\pm(a)}, \tag{5.6}$$

where the lower equilibrium is a saddle and the upper equilibrium is locally asymptotically stable. The origin remains locally stable. These facts are the inherited bistable geometry expressed as a function of $a(\ell)$.

When $a_{v1} > 0$, define the critical operator legibility

$$\boxed{\ell^\dagger = \frac{a_v^* - a_{v0}}{a_{v1}}.} \tag{5.7}$$

An interior learning-induced bifurcation is possible precisely when

$$a_{v0} < a_v^* < a_{v0} + a_{v1}, \tag{5.8}$$

so that $\ell^\dagger \in (0,1)$. If $a_{v0} > a_v^*$, persistence geometry already exists at $\ell = 0$; if $a_{v0} + a_{v1} \le a_v^*$, this learning channel cannot create it anywhere on $[0,1]$.

Above the fold, greater legibility lowers the saddle and enlarges the set of states that converge to the positive attractor. The local branch derivatives and the global comparison are proved in the Technical Appendix; the latter is the result needed downstream.

Theorem 5.1 (Nesting of the persistent basin)**.** *Let $\ell_2 > \ell_1 > \ell^\dagger$ and let $\mathcal{B}_+(\ell)$ denote the basin of attraction of the positive stable equilibrium within the interior of* $[0,1]^2$. *Then*

$$\boxed{\mathcal{B}_+(\ell_1) \subseteq \mathcal{B}_+(\ell_2).} \tag{5.9}$$

Thus increased legibility cannot make a post-withdrawal state lose membership in a previously available positive basin.

The slow and fast parts now meet at one comparison. Under the constant-summary benchmark,

$$\ell^* > \ell^\dagger \iff \eta\bar{Y}(1 - \ell^\dagger) > (\delta_\ell + \chi\bar{G})\ell^\dagger. \tag{5.10}$$

If a path starts below $\ell^\dagger$ and this inequality is strict, Theorem 4.1 implies a finite crossing into the bistable region. If the inequality fails, repeated episodes under the same environment cannot create strict bistability from below. Exact birth/loss episode indices and the reverse-learning counterpart are reported in the Technical Appendix and summarized later by the master results.

6 Experience-Dependent Transition Kernel

Cause-specific clock proofs and the general time-varying competing-risks coupling are in the Technical Appendix.

Fix one episode and compare two legibility values $0 \le \ell_1 < \ell_2 \le 1$ under identical input paths and identical initial fast states. The pressure equation (3.7) contains no ℓ, so the two counterfactuals share the same $g(t)$. For $x = (q, v, \kappa)^\top$, the remaining subsystem is cooperative on $[0,1]^3$ in the sense of Smith (1995): all off-diagonal derivatives are nonnegative, and increasing ℓ weakly increases only the v component of the vector field through $a_v(\ell)q(1-v)$.

Lemma 6.1 (Fast-path monotonicity in operator legibility)**.** *If $a_v(\ell)$ is nondecreasing, then under the matched comparison*

$$q(t;\ell_2) \ge q(t;\ell_1), \qquad v(t;\ell_2) \ge v(t;\ell_1), \qquad \kappa(t;\ell_2) \ge \kappa(t;\ell_1) \quad (t \ge 0). \tag{6.1}$$

Strict inequalities propagate after a nondegenerate interval on which the learning-sensitive visibility channel is active.

Conditional on these paths, the three substantive hazards are the attention-entry intensity (3.12), the competing fusion intensity (3.15), and the re-closure intensity (3.16). Because the baseline hazards contain no direct ℓ loading, their ordering must be transmitted through the fast states. Lemma 6.1 therefore gives

$$\lambda_A(t;\ell_2) \geq \lambda_A(t;\ell_1), \qquad \nu_F(t;\ell_2) \leq \nu_F(t;\ell_1), \qquad \mu_R(t;\ell_2) \leq \mu_R(t;\ell_1), \tag{6.2}$$

provided π is nondecreasing and the v, κ loadings in the fusion and re-closure hazards are nonnegative. For re-closure, the comparison starts from the same post-entry continuous state and the same subsequent input paths; otherwise the endogenous entry time and entry state become additional selection objects.

Definition 6.2 (Transition-improvement order)**.** *Write $\ell_2 \succeq_T \ell_1$ when the three inequalities in* (6.2) *hold under the matched comparisons. This is an order on substantive transitions, not an entrywise order on the entire transition matrix; the total exit hazard from R need not be monotone because one cause rises while the other falls.*

Theorem 6.3 (Experience-dependent transition improvement)**.** *Under the matched-path conditions above, if a_v and π are nondecreasing and the fusion/re-closure loadings on v and κ are nonnegative, then*

$$\ell_2 > \ell_1 \quad \Longrightarrow \quad \ell_2 \succeq_T \ell_1. \tag{6.3}$$

Consequently: (i) the latent cause-specific attention-entry clock is stochastically no later; (ii) at every horizon, cumulative incidence of attention as the first exit from R is weakly higher; (iii) cumulative incidence of fusion is weakly lower; and (iv) from a matched A state, first re-closure is stochastically delayed and re-closure within any fixed horizon is weakly less likely.

Two boundaries matter. First, the distribution of observed attention times conditional on attention winning the competition is selection-conditioned and is not claimed to inherit the cause-specific stochastic order. Second, re-closure from each episode's endogenous entry state is not ordered without additional assumptions. These restrictions prevent the transition theorem from silently strengthening the matched comparisons.

Combining Theorem 6.3 with the slow path gives the model's cross-episode meaning. If $\ell_0 < \ell^*$, then

$$\ell_0 \preceq_T \ell_1 \preceq_T \ell_2 \preceq_T \cdots \preceq_T \ell^*; \tag{6.4}$$

if $\ell_0 > \ell^*$ the ordering reverses. Transition improvement can therefore occur even while $\ell_n < \ell^\dagger$: easier later entry and lower fusion/re-closure are distinct from the existence of a self-sustaining post-withdrawal basin.

7 Synthesis: From Experience to the Next Transition Law

The preceding sections yield two objects that depend on the same slow state. Under a constant episode environment,

$$\ell^* = \frac{\eta \bar{Y}}{\eta \bar{Y} + \delta_\ell + \chi \bar{G}}, \tag{7.1}$$

and

$$\ell_n = \ell^* + r_\ell^n (\ell_0 - \ell^*), \qquad 0 \leq r_\ell < 1. \tag{7.2}$$

Thus ℓ_n rises, is flat, or falls according as ℓ_0 is below, at, or above ℓ^*. Section 6 established the directional transition order

$$\ell_2 > \ell_1 \Longrightarrow \lambda_A(t;\ell_2) \geq \lambda_A(t;\ell_1), \quad \nu_F(t;\ell_2) \leq \nu_F(t;\ell_1), \quad \mu_R(t;\ell_2) \leq \mu_R(t;\ell_1), \tag{7.3}$$

written $\ell_2 \succeq_T \ell_1$. Section 5 established a critical legibility $\ell^\dagger$ and, above it, nested positive persistence basins satisfying

$$\ell_2 > \ell_1 > \ell^\dagger \quad \Longrightarrow \quad \mathcal{B}_+(\ell_1) \subseteq \mathcal{B}_+(\ell_2). \tag{7.4}$$

Define the persistence-opportunity set

$$\mathcal{P}(\ell) = \begin{cases} \varnothing, & \ell \leq \ell^\dagger, \\ \mathcal{B}_+(\ell), & \ell > \ell^\dagger, \end{cases} \tag{7.5}$$

Definition 7.1 (Joint transition–geometry improvement order)**.** *For $\ell_2 > \ell_1$, write $\ell_2 \succeq_J \ell_1$ when both $\ell_2 \succeq_T \ell_1$ and $\mathcal{P}(\ell_1) \subseteq \mathcal{P}(\ell_2)$ hold.*

Proposition 7.2 (A single slow state orders both transition and geometry)**.** *Under the monotonicity conditions of Sections 6 and 5,*

$$\ell_2 > \ell_1 \quad \Longrightarrow \quad \ell_2 \succeq_J \ell_1. \tag{7.6}$$

Theorem 7.3 (Master Theorem I: experience-dependent transition improvement)**.** *Suppose $\ell_0 < \ell^*$ and the matched within-episode conditions of Section 6 hold. Then ℓ_n is nondecreasing toward ℓ^* and, for every $m > n$,*

$$\ell_m \succeq_T \ell_n. \tag{7.7}$$

Hence later episodes have a stochastically no-later cause-specific attention clock, weakly higher cumulative incidence of attention as the first resolution of R, weakly lower cumulative incidence of fusion, and weakly delayed first re-closure from a matched A state. If the fast vector field and hazards are continuous in ℓ, these finite-horizon transition objects converge to their values at ℓ^*.

The theorem orders the cause-specific attention clock and the competing cumulative incidences, not the elapsed time to *any* first exit from R. Re-closure is compared from matched post-entry states; unconditional comparisons from endogenous entry states require additional assumptions.

For geometry, let the interior critical level be

$$\ell^\dagger = \frac{a_v^* - a_{v0}}{a_{v1}}, \qquad a_v^* = \frac{4\rho d_q d_v}{(\rho - d_q)^2}, \tag{7.8}$$

and define the persistence-learning margin

$$\mathfrak{M}_P = \eta \bar{Y}(1 - \ell^\dagger) - (\delta_\ell + \chi \bar{G})\ell^\dagger. \tag{7.9}$$

Then $\mathfrak{M}_P > 0$ is equivalent to $\ell^* > \ell^\dagger$.

Theorem 7.4 (Master Theorem II: learning-induced persistence and basin expansion)**.** *Assume*

$$\ell_0 \leq \ell^\dagger. \tag{7.10}$$

If $\mathfrak{M}_P > 0$, the slow path enters the strict bistable region in finite episode time. For $0 < r_\ell < 1$, the first episode with $\ell_n > \ell^\dagger$ is

$$n_{\text{birth}} = \left\lfloor \frac{\log\{(\ell^* - \ell^\dagger)/(\ell^* - \ell_0)\}}{\log r_\ell} \right\rfloor + 1. \tag{7.11}$$

Thereafter

$$\mathcal{B}_+(\ell_n) \subseteq \mathcal{B}_+(\ell_{n+1}). \tag{7.12}$$

If $\mathfrak{M}_P \leq 0$, repetition under the same environment cannot move a path starting below the threshold into the strict bistable region; equality permits asymptotic approach but no finite crossing when $0 < r_\ell < 1$.

This result changes an opportunity set, not the realized withdrawal state. Persistence occurs only when the actual post-withdrawal state lies in the available basin.

Proposition 7.5 (Reverse-learning degradation)**.** *If $\ell_0 > \ell^*$, then ℓ_n decreases monotonically toward ℓ^* and the transition ordering reverses with episode number. If $\ell^* > \ell^\dagger$, the persistence basin remains available but shrinks toward $\mathcal{B}_+(\ell^*)$. If $\ell_0 > \ell^\dagger > \ell^*$, strict bistability is lost in finite episode time; for $0 < r_\ell < 1$ the first index with $\ell_n \leq \ell^\dagger$ is*

$$n_{\text{loss}} = \left\lceil \frac{\log\{(\ell^\dagger - \ell^*)/(\ell_0 - \ell^*)\}}{\log r_\ell} \right\rceil. \tag{7.13}$$

For brevity, write $K(\ell)$ for the within-episode transition kernel induced by legibility ℓ: the triple of intensities $(\lambda_A, \nu_F, \mu_R)(\,\cdot\,; \ell)$ together with the first-exit law they generate. Table 1 summarizes the resulting regimes. The key distinction is between improvement of the transition kernel and creation of persistence geometry: the former can occur even when $\ell^* \leq \ell^\dagger$.

Table 1: Experience-dependent regimes of the integrated model

Slow-state configuration	Learning direction	Transition kernel	Persistence geometry
$\ell_0 < \ell^* \leq \ell^\dagger$	upward	improves toward $K(\ell^*)$	no learning-induced bistability from below
$\ell_0 \leq \ell^\dagger < \ell^*$	upward	improves monotonically	born at finite n_{birth}, then basin expands
$\ell^\dagger < \ell_0 < \ell^*$	upward	improves monotonically	already present; basin expands
$\ell_0 = \ell^*$	flat	unchanged under matched conditions	unchanged
$\ell^\dagger < \ell^* < \ell_0$	downward	degrades toward $K(\ell^*)$	remains present but basin shrinks
$\ell^* < \ell^\dagger < \ell_0$	downward	degrades	lost at finite n_{loss}

8 Numerical Illustrations

The numerical examples display, rather than establish, the analytical results. The fast subsystem uses the inherited baseline vector in Table 2, $\mathcal{E}(u) = 1 - e^{-2u}$, initial condition $(q, v, g, \kappa) = (0, 0, 0, 0)$, and horizon $T = 40$. A reproduction script accompanies the manuscript and regenerates every number and figure below, including the closed-loop simulation of Section 8.5. Learning enters only through $a_v(\ell)$; the illustrative attention qualification is $\pi(\kappa) = \kappa$. Fusion and re-closure use reduced-form hazards whose absolute magnitudes are not calibrated.

Table 2: Inherited fast-system parameter vector

Symbol	Meaning	Value	Symbol	Meaning	Value
α	contact ramp-up	2.0	a_q	contact to curiosity	1.2
ρ	visibility feedback	1.5	d_q	curiosity decay	0.4
b_q	pressure inhibition	0.8	a_v	visibility formation	1.0
d_v	visibility decay	0.3	a_g	token to pressure	1.0
a_z	KPI to pressure	0.8	d_g	pressure decay	0.8
a_κ	sensitivity formation	1.2	d_κ	sensitivity decay	0.2
b_κ	pressure loss of sensitivity	0.8	λ_0	opening baseline	0.03
θ_q, θ_v	opening loadings	3.0, 1.0	θ_κ, θ_g	opening loadings	1.5, 1.0

8.1 Nestedness check

With learning fixed, $a_v = 1$, and the added fusion/re-closure channels suppressed, the model reproduces the inherited entry model, including $(q_-, v_-) = (0.1333, 0.3077)$ and $(q_+, v_+) = (0.6000, 0.6667)$. Full recovery tables and figures are in the Technical Appendix.

8.2 Set B: learning on the inherited bistable baseline

Set B keeps the inherited fast system at $\ell = 0$ and uses

$$a_v(\ell) = 1.0 + 0.8\ell, \tag{8.1}$$

with illustrative hazards

$$\nu_F = 0.12 \exp\{0.60g - 0.90v - 1.00\kappa\}, \tag{8.2}$$

$$\mu_R = 0.10 \exp\{0.50g - 0.80v - 1.00\kappa\}. \tag{8.3}$$

For entry and fusion, $u = 0.8$ and $z = 0$. Re-closure starts from the matched post-entry state $(q, v, g, \kappa) = (0.55, 0.65, 1.00, 0.30)$, with the external input held at $u = 0.8$, $z = 0$ thereafter, so that g remains at its stationary value 1 throughout the comparison. Figure 2 and Table 3 show the common-direction result: as ℓ rises from 0 to 1, median cause-specific entry time falls from 15.26 to 10.09, fusion cumulative incidence by $H = 20$ falls from 0.682 to 0.549, matched-state re-closure by $H = 10$ falls from 0.516 to 0.471, and the saddle coordinate q_- falls from 0.1333 to 0.0667.

8.3 Set C: a near-critical learning-induced bifurcation

Set C is an exogenous-summary comparative-static benchmark designed to isolate the analytical threshold mechanism; it is not asserted to be a fixed point of the endogenous episode loop examined in Set E. Because the inherited baseline is already bistable, Set C changes only the visibility mapping to

$$a_v(\ell) = 0.50 + 0.40\ell. \tag{8.4}$$

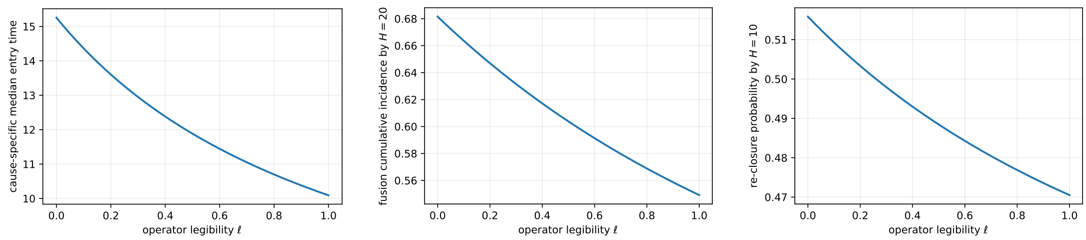

(a) Entry latency. (b) Fusion incidence. (c) Re-closure.

Figure 2: Set B: higher legibility shortens the cause-specific attention-entry clock and lowers fusion and matched-state re-closure.

Table 3: Set B: transition and geometry outcomes as operator legibility rises

ℓ	a_v	Median T_A	$C_F(20)$	$P_{RC}(10)$	q_-	q_+	v_+
0.00	1.00	15.26	0.682	0.516	0.1333	0.6000	0.6667
0.25	1.20	13.26	0.639	0.501	0.1063	0.6270	0.7149
0.50	1.40	11.88	0.604	0.488	0.0886	0.6447	0.7505
0.75	1.60	10.87	0.574	0.479	0.0761	0.6573	0.7780
1.00	1.80	10.09	0.549	0.471	0.0667	0.6667	0.8000

With $\rho = 1.5$, $d_q = 0.4$, and $d_v = 0.3$, the critical level is $a_v^* = 0.59504$ and

$$\ell^\dagger = 0.23760. \tag{8.5}$$

Using $\eta = 0.20$, $\delta_\ell = 0.03$, $\chi = 0.80$, $\ell_0 = 0.05$, $\bar{Y} = 0.40$, and $\bar{G} = 0.10$ gives $\ell^* = 0.42105$ and the path $0.0500, 0.1205, 0.1776, 0.2239, 0.2613, \ldots$. The strict bistable region is therefore entered at episode 4. Figure 4 shows the saddle-node birth and subsequent branch separation; Table 4 reports the episodes around the crossing. The episode count is illustrative, but the finite-crossing logic is the analytical result of $\ell^* > \ell^\dagger$.

Table 4: Set C: the first episodes around the bifurcation

Episode	ℓ_n	$a_v(\ell_n)$	q_-	v_-	q_+	v_+
0	0.0500	0.5200	–	–	–	–
1	0.1205	0.5482	–	–	–	–
2	0.1776	0.5710	–	–	–	–
3	0.2239	0.5895	–	–	–	–
4	0.2613	0.6045	0.3207	0.3926	0.4126	0.4540
5	0.2917	0.6167	0.2980	0.3799	0.4353	0.4723
6	0.3163	0.6265	0.2845	0.3727	0.4488	0.4838

8.4 Set D: evaluative capture and reverse learning

Holding $\bar{Y} = 0.80$ and $\ell_0 = 0.35$ fixed, changing only $\bar{G}$ yields

$$\begin{aligned} &\bar{G} = 0.10 \Rightarrow \ell^* = 0.5926, \qquad \bar{G} = 0.33393 \Rightarrow \ell^* = 0.3500, \\ &\bar{G} = 0.80 \Rightarrow \ell^* = 0.1928. \end{aligned} \tag{8.6}$$

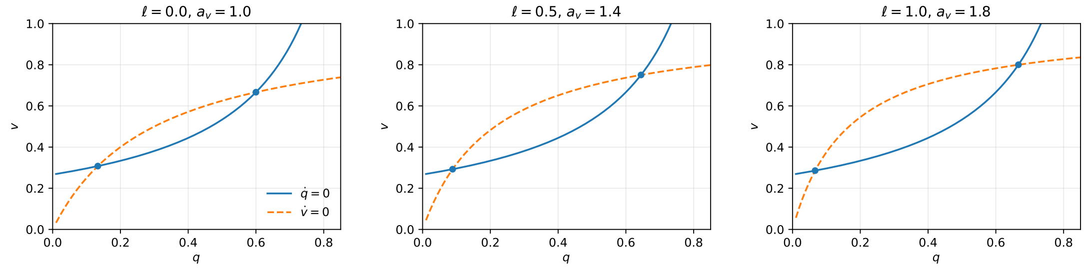

(a) $\ell = 0$.

(b) $\ell = 0.5$.

(c) $\ell = 1$.

Figure 3: Set B: on the already-bistable baseline, the saddle moves inward and the upper equilibrium outward as legibility rises.

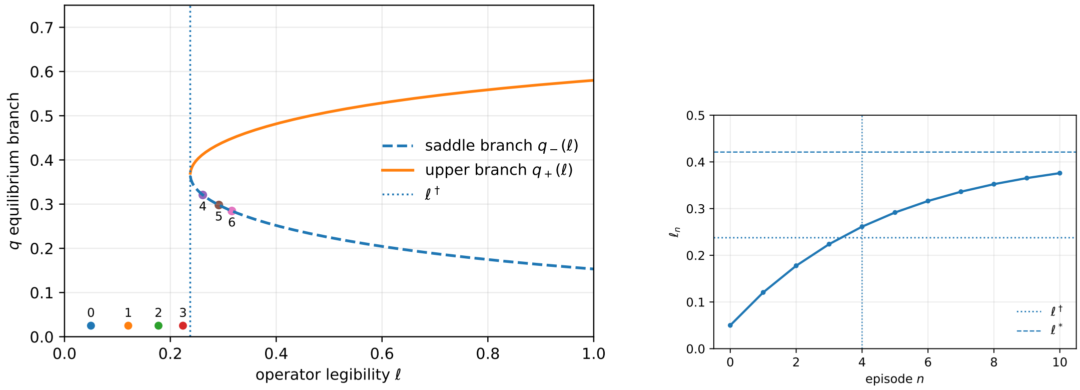

(a) Equilibrium branches.

(b) Slow crossing of $\ell^\dagger$.

Figure 4: Set C: learning-induced birth of persistence in a near-critical illustration.

Thus the same qualified-experience opportunity generates positive, flat, or reverse learning. Under the near-critical geometry of Set C, the high-evaluation path crosses below $\ell^\dagger$ and destroys a persistence opportunity that was initially available.

8.5 Set E: closing the loop—endogenous experience and path-dependent learning

Sets B–D treat the episode summaries $(\bar{Y}, \bar{G})$ as exogenous constants. Set E closes the loop of Definition 3.7: each episode's qualified experience is generated by the stochastic three-state process itself through the canonical closures (3.20)–(3.21), and the realized Y_n feeds the slow update (4.1). The fast layer, inputs, and hazards are exactly those of Sets B–C: the near-critical mapping (8.4), the illustrative hazards (8.2)–(8.3), $u = 0.8$, $z = 0$, $T_n = 40$, initial fast state $(0, 0, 0, 0)$ in every episode, and the Set C learning parameters $\eta = 0.20$, $\delta_\ell = 0.03$, $\chi = 0.80$, $\ell_0 = 0.05$, so that the only cross-episode carrier is ℓ_n. Within an episode the discrete state modulates only the accumulation of qualified exposure and does not feed back into the continuous fast equations; the Technical Appendix states this simplification explicitly. The closure constants are $\omega_Y = 1.0$ and two capture levels, $\omega_G \in \{8.7 \times 10^{-4}, 2.72 \times 10^{-3}\}$; because the pressure path is deterministic under constant inputs, G_n is the same in every episode and equals 0.033 or 0.100, the latter reproducing Set C's evaluative-capture level exactly.

Closing the loop replaces the constant $\bar{Y}$ by a random variable whose distribution

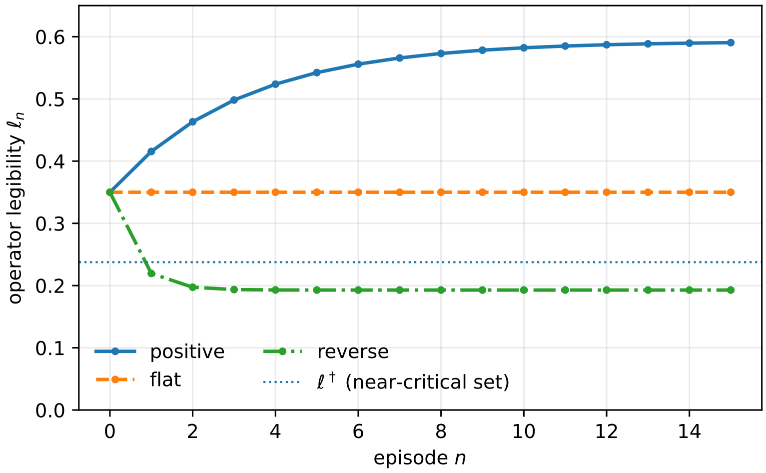

Figure 5: Set D: positive, flat, and reverse learning under the same qualified-experience opportunity. The dotted line is the near-critical $\ell^\dagger$ from Set C.

depends on ℓ_n. Simulation of $\mathbb{E}[Y \mid \ell]$ (Technical Appendix, Section S5) shows that the loop is harsher than the Set C benchmark: a qualified A spell occurs in only 13–17% of episodes over the relevant range, so the endogenously generated mean experience over the relevant legibility range is $\bar{Y}_{\text{endog}} \approx 0.09$–$0.10$, far below the $\bar{Y} = 0.40$ assumed in Set C. The mean-field analogue of the slow target is the mean-drift zero $\hat{\ell}$: the zero of the effective drift $\varphi(\ell) = \eta\,\mathbb{E}[Y \mid \ell](1-\ell) - (\delta_\ell + \chi G)\ell$, the conditional mean increment of ℓ_n. At the Set C capture level $G = 0.100$ this zero is $\hat{\ell} = 0.138 < \ell^\dagger$, so the endogenous persistence margin is negative ($\varphi(\ell^\dagger) = -0.011$) even though the exogenous margin of Set C was positive; at the milder level $G = 0.033$ the zero is $\hat{\ell} = 0.268$, just above $\ell^\dagger$ ($\varphi(\ell^\dagger) = +0.002$), so the loop is itself near critical. Both signs are decisive relative to simulation noise: direct evaluation at $\ell^\dagger$ with 200,000 episodes gives Monte Carlo standard errors below 10^{-4} for $\varphi(\ell^\dagger)$, and the 95% intervals for $\hat{\ell}$ exclude $\ell^\dagger$ at both capture levels; a still milder level $G = 0.010$ places the zero at $\hat{\ell} = 0.384$, so the three levels span negative, near-critical, and robustly positive closed-loop regimes (Technical Appendix, Section S5).

Figure 6(a) shows 40 of 4,000 simulated slow paths over 60 episodes at $G = 0.033$. Learning is punctuated rather than gradual: an episode with a qualified spell produces an upward jump of roughly $\eta Y(1-\ell) \approx 0.13$, and legibility decays geometrically between such episodes, so realized paths are sawtooth-shaped around the smooth mean-field path. The consequences are strongly path dependent under identical parameters. By episode 60, 95% of paths have crossed $\ell^\dagger$ at least once, but the first-crossing episode has median 18 with interquartile range $[10, 29]$; only 55% of paths are above $\ell^\dagger$ *at* episode 60; 90% of paths that cross subsequently fall back below the threshold at least once; and paths spend on average only 39% of episodes above it. The availability of persistence geometry is therefore intermittent rather than a one-time birth. At the Set C capture level the same statistics collapse: 84% of paths touch the threshold at least once through an occasional qualified jump, but 98% of those crossings are transient, only 14% of paths are above at episode 60, and only 12% of episode-time is spent above (Figure 6(b)). Set D's exogenous message—that the capture level decides the direction of learning—thus reappears endogenously, with the additional information that near the critical capture level individual trajectories are highly sensitive to the realized timing of rare qualified episodes.

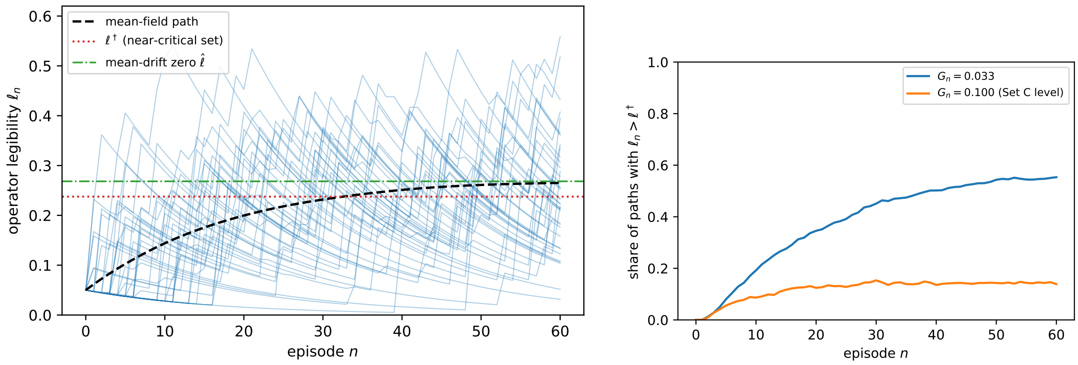

(a) Sample paths, $G_n = 0.033$.

(b) Share of paths above $\ell^\dagger$.

Figure 6: Set E: the closed loop with endogenous qualified experience. Rare qualified episodes produce jump–decay learning paths; whether and when the persistence threshold is crossed becomes path dependent, and the Set C capture level endogenously reverses the sign of the persistence margin.

Remark 8.1 (Why Set E is a simulation and not a theorem)**.** *Under the coupling of Section 6, higher legibility makes the cause-specific entry clock stochastically earlier and enlarges the pre-entry fast states, both of which push Y_n upward. A monotonicity theorem for $\mathbb{E}[Y_n \mid \ell]$ is nevertheless deliberately not claimed: the post-entry state is endogenous to the entry time, so the matched-state boundary of Theorem 6.3 blocks a pathwise inclusion of A-occupancy sets. Set E therefore illustrates a regime of the closed loop; it does not extend the ordering results. Characterizing the closed loop as a state-dependent stochastic recursion—including whether it is a monotone one—with the induced long-run distribution of ℓ_n, is a natural next analytical step; the transition and geometry theorems above are complete as a conditional transition technology and do not rest on that characterization.*

The numerical sets preserve the analytical boundaries. Set B reports a cause-specific attention clock, a competing-risk fusion incidence, and matched-state re-closure; these quantities are not interchangeable. Sets C and E are near-critical illustrations, not calibrations, and Set E's closure constants are chosen precisely to place the loop near its own critical capture level. None of the calculations identifies a human parameter, an optimal intervention, or a treatment effect. All learning-map illustrations satisfy the episode-wise step-size condition (4.2): $\eta\bar{Y} + \delta_\ell + \chi\bar{G} = 0.19$ in Set C, at most 0.83 across Set D, and $\eta Y_n + \delta_\ell + \chi G_n \leq 0.31$ in every Set E episode. All values and figures are regenerated by the accompanying script reproduce_learning_numerics.py.

9 Observable Implications

The slow state is not observationally interchangeable with current visibility. From (3.6), whenever $q > 0$ and $v < 1$,

$$a_v(\ell) = \frac{\dot{v} + d_v v}{q(1-v)}, \tag{9.1}$$

and under the affine specification (3.9),

Proposition 9.1 (Model-internal identification of operator legibility).

$$\boxed{\ell = \frac{1}{a_{v1}}\left\{\frac{\dot{v}+d_v v}{q(1-v)} - a_{v0}\right\}, \qquad a_{v1} > 0.} \tag{9.2}$$

Thus two episodes can share the same instantaneous (q, v, g, κ) *and yet have different next derivatives because their slow states differ.*

This gives a sharp lead–lag signature. At a matched instant t_0,

$$\dot{v}(t_0; \ell_2) - \dot{v}(t_0; \ell_1) = a_{v1}(\ell_2 - \ell_1)q(t_0)\{1 - v(t_0)\} > 0 \tag{9.3}$$

whenever the learning-sensitive channel is active, whereas the instantaneous derivatives of q, g, and κ are initially unchanged. The subsequent differences in q and κ arise through propagation from visibility. This separates the model from a generic claim that all favorable states simply start higher after experience.

Proposition 9.2 (State-function separation of the formation and retention channels). *Suppose the two-channel robustness specification is active, with* $a_v'(\ell) \geq 0$ *and* $d_v(\ell)$ *as in* (3.10) *(more generally* $d_v'(\ell) \leq 0$*). At a matched instant* t_0 *with state* (q, v)*,*

$$\dot{v}(t_0; \ell_2) - \dot{v}(t_0; \ell_1) = \{a_v(\ell_2) - a_v(\ell_1)\}\, q(1-v) + \{d_v(\ell_1) - d_v(\ell_2)\}\, v. \tag{9.4}$$

The formation channel loads on the state function $q(1-v)$ *and the retention channel on* v*; these state functions are linearly independent on the interior of the state square, so the two channels carry distinct empirical loadings.*

The display follows by subtracting the visibility equation at the two legibility values under the two-channel specification. The separation is at the level of state functions. Conditional on externally anchored or jointly estimated legibility values and on the parametric forms of $a_v(\cdot)$ and $d_v(\cdot)$, nondegenerate matched-state variation in (q, v) distinguishes the formation channel from the retention channel within the lead–lag design of (9.2); because ℓ is latent, linear independence of the loadings does not by itself deliver statistical identification of the full parameter vector. The two learning channels are nevertheless not observationally interchangeable: formation learning raises the visibility response most where q is high and v low, whereas retention learning raises it most where v is already high.

A second signature is bundled rather than univariate. Under comparable episodes, higher legibility predicts a faster cause-specific entry clock, less fusion as the first exit from R, and less matched-state re-closure. Evaluative capture weakens this bundle by lowering the slow target ℓ^*; near $\ell^\dagger$, gradual changes in the same slow state can additionally produce a qualitative change in post-withdrawal geometry. The model is therefore falsified in mechanism, not merely in outcome: improvement that occurs without a changed next-episode visibility response, without the predicted transition bundle, or without sensitivity to evaluative capture would favor another learning account.

These are model-implied signatures, not validated measurement procedures. Identifying ℓ, Y, and G empirically requires repeated within-person data and measurement models that preserve the distinction between current visibility and cross-episode legibility. A concrete, if demanding, design is nevertheless visible. Experience-sampling or laboratory protocols with repeated, structurally comparable self-referential inductions

Table 5: Main observable signatures and model boundaries

Model object	Predicted signature	Boundary / disconfirmation
Operator legibility	Prior qualified experience predicts the next episode's initial visibility response under matched fast state	No history effect on $\dot{v}$ when $a_{v1} > 0$ and the channel is active
Transition bundle	Entry opportunity improves while fusion and matched-state re-closure fall	Repetition improves only one outcome with no coherent fast-path change
Evaluative capture	Similar exposure can diverge because larger G lowers ℓ^*	No moderation by evaluative pressure despite variation in G
Persistence threshold	Near $\ell^\dagger$, history can change the post-withdrawal outcome through a basin shift	Smooth outcome change with no threshold-like geometry where the model predicts one
Reverse learning	If $\ell_0 > \ell^*$, repeated episodes can degrade the transition law	Improvement is imposed mechanically by episode count
Closed-loop learning	With endogenous Y_n, identically parameterized replications disperse in whether and when $\ell^\dagger$ is crossed, and crossings can be transient (Set E)	Learning curves that are deterministic functions of episode count

supply the episode structure; probe-caught reports of noticing thought *as* thought (Schooler et al., 2011) proxy current visibility v; concurrent detection of task-relevant external changes proxies object sensitivity κ; ratings of achievement framing of the observational stance itself ("trying to observe well") proxy the capture summary G; and the lead–lag signature (9.3) becomes a within-person interaction between prior qualified episodes and the early-episode visibility response at matched probe states. What such a design estimates is a measurement model built on the present state definitions; the present paper supplies the transition-law predictions that such a model would test.

10 Discussion

10.1 Learning without accumulating attention

The learned object is deliberately narrow. Operator legibility ℓ is not an attention stock, a trait-like observing capacity, or a higher-order controller. It is a slow condition on how efficiently recurrent self-referential structure becomes visible when it reappears. This distinction allows experience dependence without positing a stronger observer: the state can change while each later entry remains stochastic. It also distinguishes ℓ from current visibility v; the former changes the response law, whereas the latter is a fast state inside one episode.

The closest conceptual analogy is perceptual learning: prior experience can change how readily structure is discriminated later (Goldstone, 1998; Watanabe and Sasaki, 2015). The present model applies that idea to recurrent self-referential operator structure and gives it two downstream consequences. The same slow state orders entry/fusion/re-closure and changes post-withdrawal phase geometry. That joint consequence, rather than learning or bistability separately, is the model's substantive claim.

10.2 Why evaluative capture is central

Equation (4.1) makes repetition intrinsically ambiguous. Qualified experience forms legibility, while natural loss and evaluative capture erode it. Hence the model contains positive, flat, and reverse-learning regions without adding a separate failure process. This is important for any setting in which observation itself can become an achievement target: the same episode can supply information about recurrent structure while also increasing the pressure to succeed, monitor, or preserve an inner outcome. The sign of long-run change depends on their balance, not on exposure count alone.

The model therefore makes a stronger negative prediction than a generic learning account. When $\ell^* \leq \ell^\dagger$, the transition kernel may improve but self-sustaining geometry never becomes available from below under the maintained environment. When $\ell_0 > \ell^*$, the transition law deteriorates toward its lower target. These negative regions are not side cases; they keep the theory from reducing to "practice helps."

10.3 Entry, persistence, and re-closure are different objects

A first opening is not equivalent to durable transition. The model separates three questions: whether A occurs, whether the post-withdrawal state lies in a positive basin, and whether an A spell later re-closes. The distinction matters because the slow state can improve the transition kernel before it reaches the geometric threshold. Conversely, persistence geometry can already exist before learning. A model or experiment that uses first entry as the only outcome would therefore miss the mechanism that motivates the slow state.

The re-closure result is intentionally matched-state. Higher ℓ changes the endogenous entry time and entry state, so unconditional re-closure after each episode's own entry requires a joint coupling not proved here. Likewise, the theory orders the cause-specific attention clock and competing cumulative incidences, but not necessarily time to any first exit from R. These boundaries are mathematically substantive rather than editorial cautions.

10.4 Scope, falsifiability, and next steps

The paper is a theoretical model. It does not establish therapeutic efficacy, claim that functional non-closure is normatively superior, or show that an intervention should maximize ℓ. It also does not estimate the latent states or parameters. Its empirical burden is instead mechanistic: earlier qualified experience should predict a changed next-episode visibility response; evaluative capture should attenuate or reverse that change; the transition bundle should move in the predicted directions; and near the geometric threshold, withdrawal outcomes should display history dependence consistent with basin change.

The immediate modeling extensions are also clear. One can relax the affine $a_v(\ell)$ specification, allow legibility to affect visibility retention, or embed the episode map in continuous time; the Technical Appendix shows that the main orderings survive broad versions of these changes. Set E deliberately resets the fast state at the start of every episode so that ℓ_n is the only cross-episode carrier; allowing residual fast-state carryover—in curiosity, visibility, pressure, or object sensitivity—would introduce a second source of cross-episode history dependence and is another natural robustness extension. A further mathematical step is to treat the closed loop of Set E as a state-dependent stochastic recursion, establish whether it is monotone, and characterize the long-run distribution of ℓ_n, including conditions under which the punctuated, intermittently super-threshold regime displayed there is the typical one. A separate economic problem may value transition improvements and choose external support or withdrawal timing. That optimization is deliberately outside the present paper: the current contribution ends with a transition technology, not a welfare criterion.

11 Conclusion

This paper models a specific form of learning: an earlier qualified opening can change the law governing a later episode by changing the legibility of recurrent self-referential operators. In the fast–slow system, higher ℓ improves the matched transition kernel and enlarges the post-withdrawal persistence opportunity set; when the baseline geometry is near critical, learning can create the positive basin itself. The slow map simultaneously permits flat and reverse learning because formation competes with natural loss and evaluative capture.

The central distinction is therefore between a better current state and a changed future transition law. Attention is not stored, and entry is not guaranteed. Experience changes the conditions under which later entry, fusion, re-closure, and persistence are generated. That conditional transition architecture is the model's contribution.

Technical Appendix

When Openings Change Future Openings

Complete proofs, nestedness checks, and robustness analyses

S1 Notation for supplementary proofs

This Technical Appendix reproduces the notation needed by formal statements moved out of the main text. The definitions below are algebraically identical to the corresponding baseline model; labels are local to the Technical Appendix where the compressed main text no longer carries the auxiliary display.

For the slow map, write

$$a_n := \eta Y_n, \qquad b_n := \delta_\ell + \chi G_n, \qquad r_n := 1 - a_n - b_n, \tag{S1.1}$$

and

$$\ell_{n+1} = a_n + r_n \ell_n. \tag{S1.2}$$

The baseline discrete-time restriction is

Assumption S1.1 (Supplementary step-size condition)**.** *$\eta, \delta_\ell, \chi \geq 0$ and, for every admissible episode, $\eta Y_n + \delta_\ell + \chi G_n \leq 1$; equivalently $a_n + b_n \leq 1$, so that $r_n \in [0, 1]$. The primitive bound $\eta + \delta_\ell + \chi \leq 1$ is sufficient because $Y_n, G_n \in [0, 1]$, but it is not imposed in the numerical illustrations.*

For the constant environment,

$$Y_n \equiv \bar{Y}, \qquad G_n \equiv \bar{G}, \tag{S1.3}$$

with $a = \eta\bar{Y}$, $b = \delta_\ell + \chi\bar{G}$, $s = a + b$, $r_\ell = 1 - s$,

$$\ell^* = \frac{a}{a+b}, \qquad \ell_n = \ell^* + r_\ell^n(\ell_0 - \ell^*). \tag{S1.4}$$

We also record the threshold rearrangements

$$\bar{Y} > \frac{(\delta_\ell + \chi\bar{G})h}{\eta(1-h)}, \tag{S1.5}$$

$$\bar{G} < \frac{1}{\chi}\left\{\frac{\eta\bar{Y}(1-h)}{h} - \delta_\ell\right\}. \tag{S1.6}$$

For post-withdrawal geometry assume

Assumption S1.2 (Supplementary geometry condition)**.** *$\rho > d_q > 0$ and $d_v > 0$.*

The positive nullclines and discriminant are

$$v = \frac{aq}{d_v + aq}, \tag{S1.7}$$

$$\rho a q^2 - a(\rho - d_q)q + d_q d_v = 0, \tag{S1.8}$$

$$\Delta_h(a) = (\rho - d_q)^2 - \frac{4\rho d_q d_v}{a}. \tag{S1.9}$$

The same assumption is equivalently written $\rho > d_q > 0$, $d_v > 0$ and is referred to below as (S1.10), where

$$\rho > d_q > 0, \qquad d_v > 0. \tag{S1.10}$$

For the slow-fast coupling we use the local aliases

$$\ell^* = \frac{\eta \bar{Y}}{\eta \bar{Y} + \delta_\ell + \chi \bar{G}}, \tag{S1.11}$$

together with (S1.4).

For matched within-episode comparisons, fix identical input paths and initial fast states under $\ell_1 < \ell_2$:

Assumption S1.3 (Supplementary matched external-path comparison)**.** *$u(t), z(t)$ and $(q_0, v_0, g_0, \kappa_0)$ are identical across the two counterfactual episodes.*

The pressure equation is

$$\dot{g} = a_g u + a_z z - d_g g, \tag{S1.12}$$

and the cooperative off-diagonal terms include

$$\frac{\partial F_q}{\partial v} = \rho q(1-q) \geq 0, \tag{S1.13}$$

$$\frac{\partial F_\kappa}{\partial q} = a_\kappa v(1-\kappa) \geq 0, \qquad \frac{\partial F_\kappa}{\partial v} = a_\kappa q(1-\kappa) \geq 0. \tag{S1.14}$$

Parameter ordering enters through

$$F(t, x; \ell_2) - F(t, x; \ell_1) = \begin{bmatrix} 0 \\ \{a_v(\ell_2) - a_v(\ell_1)\} q(1-v) \\ 0 \end{bmatrix} \succeq 0. \tag{S1.15}$$

The candidate-opening, fusion, and re-closure hazards used by the moved proofs are

$$\lambda_O(t; \ell) = \lambda_0 \exp\{\theta_q q + \theta_v v + \theta_\kappa \kappa - \theta_g g\}, \tag{S1.16}$$

$$\nu_F(t; \ell) = \nu_0 \exp\{\phi_g g - \phi_v v - \phi_\kappa \kappa\}, \tag{S1.17}$$

$$\mu_R(t; \ell) = \mu_0 \exp\{\psi_g g - \psi_v v - \psi_\kappa \kappa\}. \tag{S1.18}$$

For re-closure, the matched post-entry comparison is

Assumption S1.4 (Supplementary matched post-entry comparison)**.** *The two legibility values start from the same post-entry continuous state and share the same subsequent input paths.*

If T_R is first re-closure time and $M_R(H; \ell) = \int_0^H \mu_R(s; \ell)\, ds$, then

$$\Pr\{T_R(\ell) > H\} = \exp\{-M_R(H; \ell)\}. \tag{S1.19}$$

S2 Formal statements moved out of the main text

Several auxiliary formal results are stated only in this Technical Appendix so that the main text remains compact. They are reproduced here so that the corresponding proofs and equation labels remain self-contained.

Lemma S2.1 (Positive invariance and order preservation). *Under Assumption S1.1, if* $\ell_n \in [0,1]$*, then* $\ell_{n+1} \in [0,1]$*. Moreover, for fixed* (Y_n, G_n)*, the map* $\ell \mapsto a_n + r_n \ell$ *is nondecreasing on* $[0,1]$*.*

Proposition S2.2 (Exact nonstationary solution). *For any admissible paths* $\{Y_j, G_j\}_{j \geq 0}$*, the solution of* (S1.2) *is*

$$\ell_n = \left(\prod_{j=0}^{n-1} r_j\right) \ell_0 + \sum_{k=0}^{n-1} a_k \left(\prod_{j=k+1}^{n-1} r_j\right), \qquad n \geq 1, \tag{S2.1}$$

where an empty product equals one.

Proposition S2.3 (Pathwise comparison of learning environments). *Consider two environments* H *and* L *with the same initial condition* $\ell_0^H = \ell_0^L$*. Suppose, for every episode* n*,*

$$Y_n^H \geq Y_n^L, \qquad G_n^H \leq G_n^L. \tag{S2.2}$$

Under Assumption S1.1,

$$\ell_n^H \geq \ell_n^L \qquad \text{for all } n \geq 0. \tag{S2.3}$$

Proposition S2.4 (Minimum episode count to a feasible threshold). *Assume the constant environment* (S1.3)*,* $0 < s \leq 1$*, and let* $h \in (0,1)$*. Define*

$$n_{\min}(h) := \inf\{n \in \mathbb{N}_0 : \ell_n \geq h\}.$$

Then:

(i) If $\ell_0 \geq h$*, then* $n_{\min}(h) = 0$*.*

(ii) If $\ell_0 < h < \ell^*$ *and* $0 < r_\ell < 1$*, then*

$$n_{\min}(h) = \left\lceil \frac{\log((\ell^* - h)/(\ell^* - \ell_0))}{\log r_\ell} \right\rceil. \tag{S2.4}$$

(iii) If $\ell_0 < h \leq \ell^*$ *and* $r_\ell = 0$*, then* $n_{\min}(h) = 1$*.*

(iv) If $\ell_0 < h$ *and* $h > \ell^*$*, then* $n_{\min}(h) = +\infty$*. If* $h = \ell^*$ *and* $0 < r_\ell < 1$*, the path approaches* h *asymptotically but does not reach it in finite time, so again* $n_{\min}(h) = +\infty$ *unless* $\ell_0 = h$*.*

Proposition S2.5 (Comparative statics of $\ell^\dagger$). *Suppose* $0 < \ell^\dagger < 1$ *and* $a_{v1} > 0$*. Then*

$$\frac{\partial \ell^\dagger}{\partial \rho} = -\frac{4 d_q d_v (\rho + d_q)}{a_{v1}(\rho - d_q)^3} < 0, \qquad \frac{\partial \ell^\dagger}{\partial d_q} = \frac{4 \rho d_v (\rho + d_q)}{a_{v1}(\rho - d_q)^3} > 0, \tag{S2.5}$$

$$\frac{\partial \ell^\dagger}{\partial d_v} = \frac{4 \rho d_q}{a_{v1}(\rho - d_q)^2} > 0, \qquad \frac{\partial \ell^\dagger}{\partial a_{v0}} = -\frac{1}{a_{v1}} < 0, \tag{S2.6}$$

$$\frac{\partial \ell^\dagger}{\partial a_{v1}} = -\frac{\ell^\dagger}{a_{v1}} < 0. \tag{S2.7}$$

Proposition S2.6 (Matched-fast-state history dependence). *Let two episodes have the same input paths, the same discrete state, and the same fast state at time* t_0*, but let* $\ell_2 > \ell_1$ *and* $a_{v1} > 0$*. If* $q(t_0) > 0$ *and* $v(t_0) < 1$*, then their future laws differ immediately even though their current fast states coincide.*

Additional statements stated only in the Technical Appendix

Corollary S2.7 (Ratio determines the target; scale determines speed). *Suppose $a, b > 0$. Multiplying both formation and loss by a common factor $c > 0$ such that $c(a+b) \le 1$ leaves the fixed point unchanged,*

$$\frac{ca}{ca+cb} = \ell^*,$$

but changes the retention factor from $1-(a+b)$ to $1-c(a+b)$. Thus the formation-to-loss ratio determines the long-run legibility level, whereas their common scale determines convergence speed within the non-overshooting regime.

Proposition S2.8 (Comparative statics of stationary legibility). *Assume $a > 0$ and $b > 0$. Then*

$$\frac{\partial \ell^*}{\partial \bar{Y}} = \frac{\eta b}{(a+b)^2} > 0, \qquad \frac{\partial \ell^*}{\partial \eta} = \frac{\bar{Y} b}{(a+b)^2} > 0, \tag{S2.8}$$

$$\frac{\partial \ell^*}{\partial \bar{G}} = -\frac{a\chi}{(a+b)^2} \le 0, \qquad \frac{\partial \ell^*}{\partial \delta_\ell} = -\frac{a}{(a+b)^2} < 0, \tag{S2.9}$$

$$\frac{\partial \ell^*}{\partial \chi} = -\frac{a\bar{G}}{(a+b)^2} \le 0. \tag{S2.10}$$

The inequalities involving $\bar{G}$ and χ are strict when $\chi > 0$ and $\bar{G} > 0$, respectively.

Lemma S2.9 (Positive invariance of the post-withdrawal state space). *For every fixed $\ell \in [0,1]$, the square $[0,1]^2$ is positively invariant under (5.1)–(5.2). If $q(0) > 0$, then $q(t) > 0$ for every finite $t > 0$.*

Proposition S2.10 (Complete equilibrium classification). *Under Assumption S1.2, fix $a > 0$.*

(i) The origin $E_0 = (0,0)$ is locally asymptotically stable for every $a > 0$.

(ii) If $\Delta_h(a) < 0$, there is no positive equilibrium.

(iii) If $\Delta_h(a) = 0$, there is one positive nonhyperbolic equilibrium

$$E_c = (q_c, v_c), \qquad q_c = \frac{\rho - d_q}{2\rho}, \qquad v_c = \frac{2d_q}{\rho + d_q}. \tag{S2.11}$$

It is the coalescence point of a nondegenerate saddle–node pair.

(iv) If $\Delta_h(a) > 0$, there are exactly two positive equilibria

$$q_\pm(a) = \frac{(\rho - d_q) \pm \sqrt{\Delta_h(a)}}{2\rho}, \qquad v_\pm(a) = \frac{a q_\pm(a)}{d_v + a q_\pm(a)}. \tag{S2.12}$$

The lower equilibrium $E_- = (q_-, v_-)$ is a saddle, whereas the upper equilibrium $E_+ = (q_+, v_+)$ is locally asymptotically stable.

Corollary S2.11 (Critical visibility-formation efficiency). *Under Assumption S1.2, define*

$$a_v^* := \frac{4\rho d_q d_v}{(\rho - d_q)^2}. \tag{S2.13}$$

Then the post-withdrawal system has two positive equilibria if and only if

$$a(\ell) > a_v^*. \tag{S2.14}$$

At $a(\ell) = a_v^*$ the two equilibria coalesce at E_c, and for $a(\ell) < a_v^*$ no positive equilibrium exists.

Proposition S2.12 (Three structural parameter regions)**.** *Assume $a_{v1} > 0$ and* (S1.10)*. Exactly one of the following cases holds.*

(i) ***Persistence geometry already available:*** *if $a_{v0} > a_v^*$, then $a(\ell) > a_v^*$ for every $\ell \in [0,1]$. The system is bistable throughout the admissible legibility range; learning can move the watershed but does not create the positive equilibrium pair.*

(ii) ***Learning-induced bifurcation is structurally possible:*** *if*

$$a_{v0} < a_v^* < a_{v0} + a_{v1}, \tag{S2.15}$$

then $\ell^\dagger \in (0,1)$ and

$$\ell < \ell^\dagger \Rightarrow \Delta_h < 0, \qquad \ell = \ell^\dagger \Rightarrow \Delta_h = 0, \qquad \ell > \ell^\dagger \Rightarrow \Delta_h > 0. \tag{S2.16}$$

Thus an increase in the slow state can create a saddle and a positive attractor that did not exist at lower legibility.

(iii) ***Persistence geometry is unattainable through this learning channel:*** *if $a_{v0} + a_{v1} \le a_v^*$, then no $\ell \in [0,1]$ produces two positive equilibria. Equality at $\ell = 1$ yields only the nonhyperbolic fold at the upper boundary.*

The boundary case $a_{v0} = a_v^*$ places the fold at $\ell = 0$ and yields strict bistability for every $\ell > 0$.

Proposition S2.13 (Monotone movement of the saddle and upper attractor)**.** *Assume $a_{v1} > 0$ and let ℓ lie in the bistable region $a(\ell) > a_v^*$. Then*

$$\frac{dq_-(\ell)}{d\ell} < 0, \qquad \frac{dq_+(\ell)}{d\ell} > 0, \tag{S2.17}$$

$$\frac{dv_-(\ell)}{d\ell} < 0, \qquad \frac{dv_+(\ell)}{d\ell} > 0. \tag{S2.18}$$

Moreover, the distance between the positive equilibrium branches increases with ℓ:

$$\frac{d}{d\ell}\{q_+(\ell) - q_-(\ell)\} > 0. \tag{S2.19}$$

Thus greater operator legibility moves the saddle southwest and the upper attractor northeast in the (q,v) plane.

Corollary S2.14 (Learning feasibility for the persistence threshold)**.** *Assume $0 < \ell^\dagger < 1$ and $s > 0$. Then*

$$\ell^* > \ell^\dagger \tag{S2.20}$$

if and only if

$$\eta\bar{Y}(1 - \ell^\dagger) > (\delta_\ell + \chi\bar{G})\ell^\dagger. \tag{S2.21}$$

Equivalently, when $\eta > 0$,

$$\bar{Y} > \frac{(\delta_\ell + \chi\bar{G})\ell^\dagger}{\eta(1-\ell^\dagger)}, \tag{S2.22}$$

and, when $\chi > 0$,

$$\bar{G} < \frac{1}{\chi}\left\{\frac{\eta\bar{Y}(1-\ell^\dagger)}{\ell^\dagger} - \delta_\ell\right\}. \tag{S2.23}$$

Theorem S2.15 (Learning-induced persistence geometry). *Assume the interior-threshold condition* (S2.15), $0 < s \le 1$, *and hence* $0 < \ell^\dagger < 1$.

(i) ***Upward crossing.*** *If* $\ell_0 \le \ell^\dagger < \ell^*$, *then the slow path crosses into the strict bistable region in finite episode time. If* $0 < r_\ell < 1$, *the first episode index satisfying* $\ell_n > \ell^\dagger$ *is*

$$n_{\text{birth}} = \left\lfloor \frac{\log\Big((\ell^* - \ell^\dagger)/(\ell^* - \ell_0)\Big)}{\log r_\ell} \right\rfloor + 1. \tag{S2.24}$$

If $r_\ell = 0$, *then* $n_{\text{birth}} = 1$ *unless* $\ell_0 > \ell^\dagger$ *already. For every* $n \ge n_{\text{birth}}$, *the post-withdrawal system has a saddle and a positive attractor, and their persistent basins are nested nondecreasingly as long as* ℓ_n *continues to rise.*

(ii) ***No upward crossing.*** *If* $\ell_0 \le \ell^\dagger$ *and* $\ell^* \le \ell^\dagger$, *then no finite episode enters the strict bistable region. If* $\ell^* = \ell^\dagger$ *and* $0 < r_\ell < 1$, *the fold is approached from below but not reached in finite time unless the initial state is already at the threshold.*

(iii) ***Reverse-learning loss.*** *If* $\ell_0 > \ell^\dagger > \ell^*$, *then the system begins in the bistable region but exits it in finite episode time. If* $0 < r_\ell < 1$, *the first episode index satisfying* $\ell_n \le \ell^\dagger$ *is*

$$n_{\text{loss}} = \left\lceil \frac{\log\Big((\ell^\dagger - \ell^*)/(\ell_0 - \ell^*)\Big)}{\log r_\ell} \right\rceil. \tag{S2.25}$$

If $r_\ell = 0$, *then* $n_{\text{loss}} = 1$.

If $\ell_0 > \ell^\dagger = \ell^*$ *and* $0 < r_\ell < 1$, *strict bistability survives at every finite episode but its margin converges to zero asymptotically.*

Lemma S2.16 (The pressure path is independent of legibility). *Under Assumption S1.3,*

$$g(t;\ell_2) = g(t;\ell_1) =: g(t) \qquad (t \ge 0). \tag{S2.26}$$

In particular,

$$g(t) = e^{-d_g t} g_0 + \int_0^t e^{-d_g(t-s)}\{a_g u(s) + a_z z(s)\}\, ds. \tag{S2.27}$$

Proposition S2.17 (Monotone attention-entry intensity). *Under main-text Lemma 6.1, suppose* $\theta_q, \theta_v, \theta_\kappa > 0$ *and* π *is nondecreasing. Then*

$$\lambda_O(t;\ell_2) \ge \lambda_O(t;\ell_1), \qquad \lambda_A(t;\ell_2) \ge \lambda_A(t;\ell_1) \quad (t \ge 0). \tag{S2.28}$$

If the fast-path ordering is strict on a set of positive measure in a component with positive coefficient, and $\pi(\kappa(t;\ell_2)) > 0$ *there, then the cumulative attention-entry intensity is strictly larger after that set has been traversed.*

Theorem S2.18 (Stochastic shortening of the attention-entry clock)**.** *Under Proposition S2.17,*

$$S_A(t \mid \ell_2) \leq S_A(t \mid \ell_1) \qquad (t \geq 0). \tag{S2.29}$$

Hence

$$T_A(\ell_2) \leq_{\text{st}} T_A(\ell_1), \tag{S2.30}$$

so every finite quantile of the cause-specific entry clock is weakly lower at ℓ_2. If the expectations are finite,

$$\mathbb{E}[T_A(\ell_2)] \leq \mathbb{E}[T_A(\ell_1)]. \tag{S2.31}$$

The inequalities are strict whenever the cumulative-intensity inequality is strict over a time region that affects the corresponding survival probability.

Proposition S2.19 (Monotone fusion hazard)**.** *Under main-text Lemma 6.1, suppose $\phi_v, \phi_\kappa \geq 0$. Then*

$$\nu_F(t; \ell_2) \leq \nu_F(t; \ell_1) \qquad (t \geq 0). \tag{S2.32}$$

The inequality is generated entirely by the indirect fast-path channel through v and κ; it is strict whenever a positively loaded component improves on a set of positive measure.

Theorem S2.20 (Competing-risks improvement under higher legibility)**.** *Under Propositions S2.17 and S2.19, for every horizon $t \geq 0$,*

$$C_A(t \mid \ell_2) \geq C_A(t \mid \ell_1), \qquad C_F(t \mid \ell_2) \leq C_F(t \mid \ell_1). \tag{S2.33}$$

Thus higher legibility weakly increases the probability that attention entry is the first resolution of R by any given horizon and weakly decreases the probability that fusion is the first resolution by that horizon. The same ordering holds for the ultimate first-exit probabilities whenever the limits as $t \to \infty$ exist.

Corollary S2.21 (Local stationary competing-risk formula)**.** *If over a local interval the two cause-specific hazards can be treated as constants $\bar{\lambda}_A(\ell)$ and $\bar{\nu}_F(\ell)$, the probability that fusion wins the first-exit competition is*

$$P_F(\ell) = \frac{\bar{\nu}_F(\ell)}{\bar{\lambda}_A(\ell) + \bar{\nu}_F(\ell)}, \tag{S2.34}$$

and the probability that attention wins is

$$P_A(\ell) = \frac{\bar{\lambda}_A(\ell)}{\bar{\lambda}_A(\ell) + \bar{\nu}_F(\ell)}. \tag{S2.35}$$

Whenever $\bar{\lambda}_A$ is nondecreasing and $\bar{\nu}_F$ is nonincreasing in ℓ, P_A is nondecreasing and P_F is nonincreasing.

Corollary S2.22 (Improvement in the instantaneous attention-to-fusion odds)**.** *At every time for which both hazards are positive,*

$$\frac{\lambda_A(t; \ell_2)}{\nu_F(t; \ell_2)} \geq \frac{\lambda_A(t; \ell_1)}{\nu_F(t; \ell_1)}. \tag{S2.36}$$

Thus higher legibility shifts the local resolution odds from fusion toward attention even though the total first-exit hazard $\lambda_A + \nu_F$ need not be monotone.

Proposition S2.23 (Monotone first re-closure hazard). *Under Assumption S1.4, if a_v is nondecreasing and $\psi_v, \psi_\kappa \geq 0$, then*

$$\mu_R(s; \ell_2) \leq \mu_R(s; \ell_1) \qquad (s \geq 0). \tag{S2.37}$$

Theorem S2.24 (Stochastic delay of re-closure). *Under Proposition S2.23,*

$$\Pr\{T_R(\ell_2) > H\} \geq \Pr\{T_R(\ell_1) > H\} \qquad (H \geq 0). \tag{S2.38}$$

Equivalently,

$$T_R(\ell_2) \geq_{\mathrm{st}} T_R(\ell_1). \tag{S2.39}$$

The probability of re-closure within a horizon H,

$$P_{RC}(H \mid \ell) = 1 - \exp\{-M_R(H; \ell)\}, \tag{S2.40}$$

is therefore weakly decreasing in ℓ. If the expected A-spell lengths are finite, $\mathbb{E}[T_R(\ell)]$ is weakly increasing in ℓ.

Corollary S2.25 (Structural-path sufficiency for fusion and re-closure). *If $a_v(\ell_2) > a_v(\ell_1)$ and the interior activation conditions of Lemma 6.1 generate strict increases in v or κ on sets of positive measure, then fusion and re-closure hazards fall strictly whenever the corresponding coefficients ϕ_v, ϕ_κ or ψ_v, ψ_κ place positive weight on a strictly improved state. No direct legibility loading is required.*

S3 Complete proofs of formal results

The main text states the central formal results and reports their implications. This Technical Appendix collects the complete proofs. Cross-references of the form "Main text" point to numbered results of the main text; all other numbered references are internal to the Technical Appendix.

Proof of Positive invariance and order preservation (technical-appendix result, S2.1)

Proof. Equation (S1.2) is affine in ℓ. At the endpoints,

$$\mathcal{L}_n(0) = a_n \in [0,1], \qquad \mathcal{L}_n(1) = 1 - b_n \in [0,1].$$

An affine map takes the interval $[0,1]$ into the interval spanned by its endpoint images, so $\mathcal{L}_n([0,1]) \subseteq [0,1]$. Its derivative with respect to ℓ is $r_n \geq 0$, which gives order preservation. $\square$

Proof of Exact nonstationary solution (technical-appendix result, S2.2)

Proof. The claim follows by repeated substitution. For $n = 1$, (S2.1) gives $\ell_1 = r_0\ell_0 + a_0$. Suppose the formula holds at n. Then

$$\begin{aligned}
\ell_{n+1} &= a_n + r_n\ell_n \\
&= a_n + r_n\left(\prod_{j=0}^{n-1} r_j\right)\ell_0 + r_n\sum_{k=0}^{n-1} a_k\left(\prod_{j=k+1}^{n-1} r_j\right) \\
&= \left(\prod_{j=0}^{n} r_j\right)\ell_0 + \sum_{k=0}^{n} a_k\left(\prod_{j=k+1}^{n} r_j\right),
\end{aligned}$$

which is the formula at $n + 1$. □

Proof of Pathwise comparison of learning environments (technical-appendix result, S2.3)

Proof. For any $\ell \in [0, 1]$, the one-step map satisfies

$$\frac{\partial \mathcal{L}}{\partial Y} = \eta(1 - \ell) \geq 0, \qquad \frac{\partial \mathcal{L}}{\partial G} = -\chi\ell \leq 0.$$

Hence (S2.2) implies $\mathcal{L}_n^H(\ell) \geq \mathcal{L}_n^L(\ell)$ for every ℓ. By Lemma S2.1, each map is nondecreasing in its state argument. If $\ell_n^H \geq \ell_n^L$, then

$$\ell_{n+1}^H = \mathcal{L}_n^H(\ell_n^H) \geq \mathcal{L}_n^H(\ell_n^L) \geq \mathcal{L}_n^L(\ell_n^L) = \ell_{n+1}^L.$$

Induction from the common initial condition proves the result. □

Proof of Global monotone convergence of the slow map (Main text, 4.1)

Proof. If $s = 0$, nonnegativity of a and b implies $a = b = 0$, so (S1.2) is the identity map.

Now suppose $0 < s \leq 1$. A fixed point satisfies $\ell = a + (1 - s)\ell$, or $s\ell = a$, giving the unique fixed point $\ell^* = a/s$. Subtracting ℓ^* from the recurrence gives

$$\ell_{n+1} - \ell^* = r_\ell(\ell_n - \ell^*).$$

Iteration yields (4.5). Because $0 \leq r_\ell < 1$, $r_\ell^n \to 0$, so $\ell_n \to \ell^*$. Also

$$\ell_{n+1} - \ell_n = s(\ell^* - \ell_n). \tag{S3.1}$$

Hence the increment is positive below ℓ^*, negative above it, and zero at it. This proves monotonicity. If $0 < r_\ell < 1$ and $\ell_n \neq \ell^*$, the inequality is strict. When $r_\ell = 0$ ($s = 1$), the map reaches ℓ^* in one step. □

Proof of Comparative statics of stationary legibility (technical-appendix result, S2.8)

Proof. Differentiate (4.4) using $a = \eta\bar{Y}$ and $b = \delta_\ell + \chi\bar{G}$. □

Proof of Threshold-feasibility condition (Main text, 4.2)

Proof. From (4.4), $\ell^* > h$ is equivalent to

$$\eta\bar{Y} > h\{\eta\bar{Y} + \delta_\ell + \chi\bar{G}\},$$

which rearranges to (4.7). Solving the same inequality for $\bar{Y}$ or $\bar{G}$ gives (S1.5) and (S1.6). □

Proof of Minimum episode count to a feasible threshold (technical-appendix result, S2.4)

Proof. Part (i) is immediate from the definition. For part (ii), Theorem 4.1 gives

$$\ell^* - \ell_n = r_\ell^n(\ell^* - \ell_0).$$

Because $\ell_0 < h < \ell^*$, the ratio

$$\zeta := \frac{\ell^* - h}{\ell^* - \ell_0}$$

lies in $(0, 1)$. The condition $\ell_n \geq h$ is equivalent to $r_\ell^n \leq \zeta$. Taking logarithms and using $\log r_\ell < 0$ gives

$$n \geq \frac{\log \zeta}{\log r_\ell}.$$

The smallest integer satisfying the inequality is (S2.4). If $r_\ell = 0$, one step sends every initial state to ℓ^*, proving part (iii). For part (iv), monotone convergence from below implies $\ell_n < \ell^*$ for every finite n when $0 < r_\ell < 1$, so a threshold above ℓ^* is impossible and the threshold equal to ℓ^* is only approached asymptotically. □

Proof of Positive invariance of the post-withdrawal state space (technical-appendix result, S2.9)

Proof. On $q = 0$, $\dot{q} = 0$. On $q = 1$, $\dot{q} = -d_q < 0$. On $v = 0$, $\dot{v} = a(\ell)q \geq 0$, and on $v = 1$, $\dot{v} = -d_v < 0$. Thus the vector field points inward or is tangent on every face of the square. Moreover, (5.1) has the multiplicative form $\dot{q} = q\,H(q, v)$ with continuous H, so a solution starting from $q(0) > 0$ cannot reach $q = 0$ in finite time. □

Proof of Complete equilibrium classification (technical-appendix result, S2.10)

Proof. At the origin the Jacobian is

$$J(E_0) = \begin{bmatrix} -d_q & 0 \\ a & -d_v \end{bmatrix},$$

whose eigenvalues are $-d_q$ and $-d_v$.

For positive equilibria, (S1.8) is a quadratic in q with discriminant $a^2\Delta_h(a)$. Hence there are zero, one double, or two positive roots according as $\Delta_h(a)$ is negative, zero, or positive. Under $\rho > d_q$, the sum of the two roots when they exist is $(\rho - d_q)/\rho \in (0, 1)$ and their product is $d_q d_v/(\rho a) > 0$, so both roots lie in $(0, 1)$. Equation (S1.7) then places the associated v values in $(0, 1)$.

When $\Delta_h(a) = 0$, the double root is $q_c = (\rho - d_q)/(2\rho)$. Substitution into either nullcline gives $v_c = 2d_q/(\rho + d_q)$.

It remains to classify the positive equilibria. Write

$$f(q, v) = q\{\rho v(1 - q) - d_q\}, \qquad g(q, v) = aq(1 - v) - d_v v.$$

At any positive equilibrium the trace satisfies

$$\operatorname{tr} J = -\rho v q - (aq + d_v) < 0. \tag{S3.2}$$

To determine the determinant, use the reduced positive-equilibrium equation. Since $g_v = -(aq + d_v) < 0$, the implicit function theorem gives the v-nullcline $v = V(q; a)$. Define

$$R(q; a) := \rho V(q; a)(1 - q) - d_q = \frac{h(q; a)}{d_v + aq}.$$

At a positive equilibrium, $f = qR$ and $R = 0$. A direct calculation gives

$$\det J = q\, g_v\, R_q.$$

Because $h = 0$ at an equilibrium,

$$R_q = \frac{h_q}{d_v + aq}, \qquad h_q = a\{(\rho - d_q) - 2\rho q\}.$$

Thus $h_q > 0$ at q_- and $h_q < 0$ at q_+. Since $q > 0$ and $g_v < 0$, $\det J < 0$ at E_-, proving that E_- is a saddle. At E_+, $\det J > 0$ and the trace is negative, so E_+ is locally asymptotically stable.

At $\Delta_h(a) = 0$, $h_q(q_c; a) = 0$, so one eigenvalue is zero while the other equals the negative trace. The equilibrium equation has a nondegenerate fold. Indeed, at the critical point,

$$h_{qq} = -2\rho a < 0,$$

and

$$h_a = q\{(\rho - d_q) - \rho q\} \quad \Longrightarrow \quad h_a(q_c; a) = \frac{q_c(\rho - d_q)}{2} > 0.$$

Because $g_v \neq 0$, the two-dimensional equilibrium problem is locally reducible to the scalar equation $R(q; a) = 0$, for which $R_q = 0$, $R_{qq} \neq 0$, and $R_a \neq 0$ at the critical point. Hence the coalescence is a nondegenerate saddle–node. □

Proof of Critical visibility-formation efficiency (technical-appendix result, S2.11)

Proof. By (S1.9), $\Delta_h(a) > 0$ is equivalent to

$$(\rho - d_q)^2 > \frac{4\rho d_q d_v}{a},$$

which is equivalent to $a > a_v^*$. □

Proof of Three structural parameter regions (technical-appendix result, S2.12)

Proof. Because $a(\ell) = a_{v0} + a_{v1}\ell$ is strictly increasing, its range on $[0,1]$ is $[a_{v0}, a_{v0} + a_{v1}]$. The claims follow immediately by comparing this interval with the critical value a_v^* and using Corollary S2.11. In the interior case, solving $a(\ell) = a_v^*$ gives (5.7), and strict monotonicity gives (S2.16). $\square$

Proof of Monotone movement of the saddle and upper attractor (technical-appendix result, S2.13)

Proof. Write

$$\Delta_h(\ell) = (\rho - d_q)^2 - \frac{4\rho d_q d_v}{a(\ell)}.$$

Since $a'(\ell) = a_{v1} > 0$,

$$\Delta_h'(\ell) = \frac{4\rho d_q d_v\, a_{v1}}{a(\ell)^2} > 0. \tag{S3.3}$$

Differentiating

$$q_\pm(\ell) = \frac{(\rho - d_q) \pm \sqrt{\Delta_h(\ell)}}{2\rho}$$

gives

$$q_-'(\ell) = -\frac{\Delta_h'(\ell)}{4\rho\sqrt{\Delta_h(\ell)}} < 0, \qquad q_+'(\ell) = \frac{\Delta_h'(\ell)}{4\rho\sqrt{\Delta_h(\ell)}} > 0. \tag{S3.4}$$

At every positive equilibrium, the q-nullcline gives

$$v_\pm(\ell) = \frac{d_q}{\rho\{1 - q_\pm(\ell)\}}.$$

The right-hand side is strictly increasing in q, so v_-' and v_+' have the same signs as q_-' and q_+', respectively. Finally,

$$q_+ - q_- = \frac{\sqrt{\Delta_h}}{\rho},$$

whose derivative is positive by (S3.3). $\square$

Proof of Nesting of the persistent basin (Main text, 5.1)

Proof. Let $a_i = a(\ell_i)$, so $a_2 > a_1$. First observe that the system is cooperative on $[0,1]^2$: the off-diagonal derivatives satisfy

$$\frac{\partial \dot q}{\partial v} = \rho q(1-q) \geq 0, \qquad \frac{\partial \dot v}{\partial q} = a(1-v) \geq 0.$$

It is also ordered in the parameter a because $\partial \dot q/\partial a = 0$ and

$$\frac{\partial \dot v}{\partial a} = q(1-v) \geq 0.$$

Therefore, for the same initial condition $x_0 = (q_0, v_0)$, solutions satisfy

$$x(t; a_2) \geq x(t; a_1) \quad \text{componentwise for all } t \geq 0. \tag{S3.5}$$

For completeness, the order follows from a first-contact argument. On the boundary of the difference cone $q_2 - q_1 \geq 0$, $v_2 - v_1 \geq 0$, if $q_2 = q_1 = q$ then

$$\dot{q}_2 - \dot{q}_1 = \rho q(1-q)(v_2 - v_1) \geq 0,$$

and if $v_2 = v_1 = v$ then

$$\dot{v}_2 - \dot{v}_1 = (a_2 q_2 - a_1 q_1)(1-v) \geq 0$$

whenever $q_2 \geq q_1$. Hence the difference cannot cross out of the nonnegative cone.

Second, no periodic orbit lies in the positive interior. The Dulac function $B(q,v) = 1/q$ gives

$$\frac{\partial}{\partial q}\{B\dot{q}\} + \frac{\partial}{\partial v}\{B\dot{v}\} = -\rho v - a - \frac{d_v}{q} < 0$$

throughout $(0,1)^2$. Thus the Bendixson–Dulac criterion excludes periodic orbits there. The same inequality excludes closed graphics: along a homoclinic loop or heteroclinic cycle the vector field is tangent to the curve (and vanishes at the equilibria on it), so the outward flux of $B\,(\dot{q},\dot{v})$ through the curve is zero, while Green's theorem equates that flux to the integral of the displayed negative divergence over the enclosed region—a contradiction. By the planar Poincaré–Bendixson theorem on the compact positively invariant square, every omega-limit set is therefore a single equilibrium. Hence every positive trajectory converges to one of the finitely many equilibria; points on the stable manifold of the saddle converge to the saddle itself.

Now take $x_0 \in \mathcal{B}_+(\ell_1)$. Then

$$x(t;a_1) \longrightarrow E_+(a_1).$$

By (S3.5), every accumulation point of $x(t;a_2)$ is componentwise at least $E_+(a_1)$. Proposition S2.13 gives

$$E_-(a_2) < E_-(a_1) < E_+(a_1) < E_+(a_2)$$

componentwise. Hence the a_2 trajectory cannot converge to the origin or to $E_-(a_2)$. Since no periodic attractor exists, it must converge to $E_+(a_2)$. Therefore $x_0 \in \mathcal{B}_+(\ell_2)$, proving (5.9). □

Proof of Comparative statics of $\ell^\dagger$ (technical-appendix result, S2.5)

Proof. Differentiate

$$a_v^* = \frac{4\rho d_q d_v}{(\rho - d_q)^2}.$$

One obtains

$$\frac{\partial a_v^*}{\partial \rho} = -\frac{4 d_q d_v(\rho + d_q)}{(\rho - d_q)^3}, \quad \frac{\partial a_v^*}{\partial d_q} = \frac{4\rho d_v(\rho + d_q)}{(\rho - d_q)^3}, \quad \frac{\partial a_v^*}{\partial d_v} = \frac{4\rho d_q}{(\rho - d_q)^2}.$$

Since $\ell^\dagger = (a_v^* - a_{v0})/a_{v1}$, the first four derivatives follow directly. For the final derivative,

$$\frac{\partial \ell^\dagger}{\partial a_{v1}} = -\frac{a_v^* - a_{v0}}{a_{v1}^2} = -\frac{\ell^\dagger}{a_{v1}}.$$

□

Proof of Learning feasibility for the persistence threshold (technical-appendix result, S2.14)

Proof. Substitute (S1.11) into $\ell^* > \ell^\dagger$ and rearrange. The threshold forms follow by solving the same strict inequality for $\bar{Y}$ and $\bar{G}$. □

Proof of Learning-induced persistence geometry (technical-appendix result, S2.15)

Proof. Under $0 < s \leq 1$, Section 4 gives (S1.4) and monotone movement toward ℓ^*. For part (i), suppose first $0 < r_\ell < 1$. Because $\ell_0 \leq \ell^\dagger < \ell^*$, the condition $\ell_n > \ell^\dagger$ is equivalent to

$$r_\ell^n < \frac{\ell^* - \ell^\dagger}{\ell^* - \ell_0} =: \zeta, \qquad 0 < \zeta \leq 1.$$

Taking logarithms and using $\log r_\ell < 0$ gives

$$n > \frac{\log \zeta}{\log r_\ell}.$$

The smallest integer satisfying the strict inequality is (S2.24). If $r_\ell = 0$, one episode sends the state to $\ell^* > \ell^\dagger$. Proposition S2.12 then gives bistability for all subsequent episodes, and Theorem 5.1 gives basin nesting along the increasing path.

For part (ii), monotone convergence to a target at or below $\ell^\dagger$ prevents an upward crossing. When the target equals the threshold and $0 < r_\ell < 1$, (S1.4) shows $\ell_n < \ell^\dagger$ at every finite n if the path begins below it.

For part (iii), ℓ_n decreases monotonically toward ℓ^*. With $0 < r_\ell < 1$, the condition $\ell_n \leq \ell^\dagger$ is equivalent to

$$r_\ell^n \leq \frac{\ell^\dagger - \ell^*}{\ell_0 - \ell^*} =: \xi, \qquad 0 < \xi < 1.$$

Taking logarithms gives

$$n \geq \frac{\log \xi}{\log r_\ell},$$

and the smallest integer satisfying this weak inequality is (S2.25). If $r_\ell = 0$, the state jumps to $\ell^* < \ell^\dagger$ in one episode. Finally, if $\ell^* = \ell^\dagger < \ell_0$ with $0 < r_\ell < 1$, then

$$\ell_n - \ell^\dagger = r_\ell^n(\ell_0 - \ell^\dagger) > 0$$

for every finite n, while the difference converges to zero. □

Proof of The pressure path is independent of legibility (technical-appendix result, S2.16)

Proof. Equation (S1.12) contains neither ℓ nor the other fast states. With the same initial condition and the same inputs it therefore has the same unique solution in the two counterfactual episodes. Variation of constants gives (S2.27). □

Proof of Fast-path monotonicity in operator legibility (Main text, 6.1)

Proof. Equations (S1.13)–(S1.14) show that F is quasimonotone nondecreasing in the state. Equation (S1.15) shows that the vector field under ℓ_2 weakly dominates the vector field under ℓ_1 at every common state and time. The standard comparison argument for cooperative ODEs (e.g., Smith, 1995) therefore gives (6.1) from the common initial condition.

For strictness, if $a_v(\ell_2) > a_v(\ell_1)$ and $q > 0$, $v < 1$ on a nondegenerate interval, then the second component of (S1.15) is strictly positive there. Hence $v(t; \ell_2) > v(t; \ell_1)$ after that interval. A strict increase in v raises the q vector field by $\rho q(1-q)\Delta v$ whenever $0 < q < 1$, creating strict q ordering thereafter. Finally, the κ vector field is strictly increasing in either q or v when the other multiplicative terms are positive and $\kappa < 1$. Uniqueness prevents the strictly ordered trajectories from crossing back through equality once the relevant strict inequality has propagated. □

Proof of Monotone attention-entry intensity (technical-appendix result, S2.17)

Proof. By Lemma S2.16, the $-\theta_g g(t)$ term is identical across the two episodes. Lemma 6.1 makes each of q, v, κ weakly larger under ℓ_2, so the exponential factor in (S1.16) is weakly larger. This proves the first inequality. Because π is nondecreasing, $\pi(\kappa(t; \ell_2)) \geq \pi(\kappa(t; \ell_1))$, proving the second. Strictness of the cumulative intensity follows when the pointwise inequality is strict on a set of positive measure. □

Proof of Stochastic shortening of the attention-entry clock (technical-appendix result, S2.18)

Proof. Proposition S2.17 implies $\Lambda_A(t; \ell_2) \geq \Lambda_A(t; \ell_1)$ for every t. Exponentiation with a negative sign gives (S2.29), which is exactly first-order stochastic dominance in the direction (S2.30). Quantile ordering follows from first-order stochastic dominance. If the means are finite, use the tail-integral identity

$$\mathbb{E}[T_A(\ell)] = \int_0^\infty S_A(t \mid \ell)\, dt$$

and integrate (S2.29). □

Proof of Monotone fusion hazard (technical-appendix result, S2.19)

Proof. The pressure term $\phi_g g(t)$ is identical by Lemma S2.16. The remaining terms in the exponent of (S1.17) are nonpositive multiples of v and κ, both of which weakly increase with ℓ. Therefore the exponent, and hence the exponential hazard, weakly decreases. □

Proof of Competing-risks improvement under higher legibility (technical-appendix result, S2.20)

Proof. Let E_A, E_F be independent unit-exponential random variables on a common probability space. For $j \in \{1, 2\}$ define the latent clocks

$$\tau_A^{(j)} := \inf\{t \geq 0 : \Lambda_A(t; \ell_j) \geq E_A\},$$
$$\tau_F^{(j)} := \inf\{t \geq 0 : \Lambda_F(t; \ell_j) \geq E_F\},$$

with the usual convention that the infimum is ∞ if the threshold is never reached. Proposition S2.17 implies

$$\Lambda_A(t; \ell_2) \geq \Lambda_A(t; \ell_1) \quad \Rightarrow \quad \tau_A^{(2)} \leq \tau_A^{(1)}$$

pathwise. Proposition S2.19 implies

$$\Lambda_F(t; \ell_2) \leq \Lambda_F(t; \ell_1) \quad \Rightarrow \quad \tau_F^{(2)} \geq \tau_F^{(1)}$$

pathwise.

If attention wins by time t under ℓ_1, then

$$\tau_A^{(1)} \leq t, \qquad \tau_A^{(1)} < \tau_F^{(1)}.$$

The pathwise inequalities give

$$\tau_A^{(2)} \leq \tau_A^{(1)} < \tau_F^{(1)} \leq \tau_F^{(2)},$$

so attention also wins by time t under ℓ_2. Hence the event defining $C_A(t \mid \ell_1)$ is a subset of the event defining $C_A(t \mid \ell_2)$.

Conversely, if fusion wins by time t under ℓ_2, then

$$\tau_F^{(2)} \leq t, \qquad \tau_F^{(2)} < \tau_A^{(2)}.$$

Since $\tau_F^{(1)} \leq \tau_F^{(2)} < \tau_A^{(2)} \leq \tau_A^{(1)}$, fusion also wins by time t under ℓ_1. Hence the fusion event under ℓ_2 is a subset of the fusion event under ℓ_1. Taking probabilities proves (S2.33). The infinite-horizon result follows by monotone limits. □

Proof of Local stationary competing-risk formula (technical-appendix result, S2.21)

Proof. The formulas are the standard two-clock probabilities for constant hazards. Differentiating (S2.34) gives

$$P_F'(\ell) = \frac{\bar{\nu}_F' \bar{\lambda}_A - \bar{\nu}_F \bar{\lambda}_A'}{(\bar{\lambda}_A + \bar{\nu}_F)^2} \leq 0,$$

and $P_A = 1 - P_F$. □

Proof of Improvement in the instantaneous attention-to-fusion odds (technical-appendix result, S2.22)

Proof. The numerator is weakly larger and the denominator weakly smaller under ℓ_2. $\square$

Proof of Monotone first re-closure hazard (technical-appendix result, S2.23)

Proof. The matched post-entry comparison is mathematically identical to the matched episode comparison used in Lemmas S2.16 and 6.1. Thus the pressure paths are identical and (q, v, κ) are weakly larger under ℓ_2. Every fast-state term in the exponent of (S1.18) therefore weakly lowers the hazard under ℓ_2. $\square$

Proof of Stochastic delay of re-closure (technical-appendix result, S2.24)

Proof. Proposition S2.23 implies $M_R(H; \ell_2) \leq M_R(H; \ell_1)$ for every H. Apply the exponential survival map in (S1.19). The stochastic order, the monotonicity of (S2.40), and the mean ordering follow exactly as in Theorem S2.18. $\square$

Proof of Experience-dependent transition improvement (Main text, 6.3)

Proof. Lemma 6.1 gives the state-path order. Proposition S2.17 converts that order into $\lambda_A(\ell_2) \geq \lambda_A(\ell_1)$. Proposition S2.19 gives $\nu_F(\ell_2) \leq \nu_F(\ell_1)$, and Proposition S2.23 gives $\mu_R(\ell_2) \leq \mu_R(\ell_1)$. This proves (6.3). The four consequences are Theorems S2.18, S2.20, and S2.24. $\square$

Proof of Structural-path sufficiency for fusion and re-closure (technical-appendix result, S2.25)

Proof. The only differences in the exponents of (S1.17) and (S1.18) come through the fast states because g is common. Strict state improvement in a component with a positive negative-loading coefficient therefore makes the relevant exponent strictly smaller on the corresponding set of positive measure. $\square$

Proof of A single slow state orders both transition and geometry (Main text, 7.2)

Proof. The transition component follows from (7.3). For the geometry component there are three cases. If $\ell_2 \leq \ell^\dagger$, both persistence-opportunity sets are empty. If $\ell_1 \leq \ell^\dagger < \ell_2$, then $\mathcal{P}(\ell_1) = \varnothing \subseteq \mathcal{P}(\ell_2)$. If $\ell^\dagger < \ell_1 < \ell_2$, inclusion follows from (7.4). Hence both components of Definition 7.1 hold. $\square$

Proof of Master Theorem I: experience-dependent transition improvement (Main text, 7.3)

Proof. Part (i) follows from the exact learning path (7.2): with $\ell_0 < \ell^*$ and $0 \leq r_\ell < 1$, the sequence moves monotonically toward ℓ^*. Part (ii) follows by applying (7.3) to every pair $\ell_m \geq \ell_n$, with strict legibility inequality when the slow path is strictly increasing. The stochastic consequences are the entry-clock, competing-risks, and re-closure orderings established by the transition-kernel analysis.

For part (iii), fix a finite horizon $[0, T]$. The fast vector field is locally Lipschitz in the state variables on the compact invariant state set and continuous in the parameter ℓ. Standard continuous dependence of ODE solutions on parameters therefore gives uniform convergence of the fast state paths as $\ell_n \to \ell^*$. The hazard functions are continuous compositions of those state paths and ℓ, so they converge uniformly as well. Integrals of the hazards over $[0, T]$ converge, and therefore so do the finite-horizon survival functions and cumulative-incidence functionals constructed from those integrated hazards. □

Proof of Master Theorem II (Main text, 7.4)

Proof. The equivalence between $\mathfrak{M}_P > 0$ and $\ell^* > \ell^\dagger$ follows by substituting (7.1) and rearranging. Under a positive margin and (7.10), the exact path (7.2) rises monotonically toward a target above $\ell^\dagger$, so it crosses the threshold in finite time. Solving $\ell_n > \ell^\dagger$ for the smallest integer n yields (7.11). Once the path is above the threshold, the equilibrium-classification result gives the saddle and positive attractor, while basin nesting gives (7.12). If $\ell^* \leq \ell^\dagger$, monotone convergence from a starting point at or below the threshold cannot produce an upward crossing. The equality case follows directly from the geometric convergence formula (7.2). □

Proof of Reverse-learning degradation (Main text, 7.5)

Proof. The slow-map direction follows from (7.2). Since the transition and persistence orders are monotone in ℓ, a decreasing sequence reverses the episode ordering. If the target remains above $\ell^\dagger$, every state on the monotone path remains above the threshold and basin nesting applies in the reverse direction. If the target lies below $\ell^\dagger$ while the initial state lies above it, monotone convergence forces a finite downward crossing. Solving $\ell_n \leq \ell^\dagger$ gives (7.13). □

Proof of Matched-fast-state history dependence (technical-appendix result, S2.6)

Proof. At the matched state, the only fast equation with a direct ℓ dependence in the central specification is the visibility equation. Hence

$$\dot{v}(t_0; \ell_2) - \dot{v}(t_0; \ell_1) = a_{v1}(\ell_2 - \ell_1) q(t_0)\{1 - v(t_0)\} > 0. \tag{S3.6}$$

At the same instant, $\dot{q}$, $\dot{g}$, and $\dot{\kappa}$ are equal because their right-hand sides have no direct ℓ term when the fast states and inputs are matched. The trajectories therefore begin to separate through v, after which the coupling of v into q and κ propagates the difference through the fast system and the transition intensities. □

Proof of Positive invariance of the fast state space (technical-appendix result, S6.1)

Proof. The vector field points inward on every boundary face. At $q = 0$, $\dot{q} = a_q \mathcal{E}(u) \geq 0$; at $q = 1$, $\dot{q} = -(d_q + b_q g) \leq 0$. At $v = 0$, $\dot{v} = a_v(\ell) q \geq 0$; at $v = 1$, $\dot{v} = -d_v(\ell) \leq 0$. At $\kappa = 0$, $\dot{\kappa} = a_\kappa q v \geq 0$; at $\kappa = 1$, $\dot{\kappa} = -(d_\kappa + b_\kappa g) \leq 0$. Finally, at $g = 0$,

$\dot{g} = a_g u + a_z z \geq 0$. A first-exit argument therefore rules out departure from the stated domain. $\square$

Proof of Generalized matched-path comparison (technical-appendix result, S6.2)

Proof. The pressure equation (S6.3) is independent of ℓ, q, v, κ, so the two g paths coincide. Fix this common path and let $x = (q, v, \kappa)$. The subsystem is cooperative because its off-diagonal derivatives are

$$\frac{\partial \dot{q}}{\partial v} = \rho q(1-q) \geq 0, \qquad \frac{\partial \dot{v}}{\partial q} = a_v(\ell)(1-v) \geq 0,$$

$$\frac{\partial \dot{\kappa}}{\partial q} = a_\kappa v(1-\kappa) \geq 0, \qquad \frac{\partial \dot{\kappa}}{\partial v} = a_\kappa q(1-\kappa) \geq 0.$$

At a common state x, only the v component changes directly with ℓ, and

$$\dot{v}(x;\ell_2) - \dot{v}(x;\ell_1) = \{a_v(\ell_2) - a_v(\ell_1)\}q(1-v) \tag{S3.7}$$
$$+ \{d_v(\ell_1) - d_v(\ell_2)\}v \geq 0. \tag{S3.8}$$

Suppose that the componentwise order first failed at time t^*. At the first contact of the difference process with a boundary of the nonnegative cone, the derivative of the zero component cannot point outward: if $q_2 = q_1$, its derivative difference is $\rho q(1-q)(v_2 - v_1) \geq 0$; if $v_2 = v_1$, the derivative difference is nonnegative by (S3.8) together with $q_2 \geq q_1$; and if $\kappa_2 = \kappa_1$, its derivative difference is nonnegative because the κ vector field is increasing in both q and v. Hence no first outward crossing exists, proving (S6.6). $\square$

Proof of Monotone competing-risks coupling (technical-appendix result, S7.1)

Proof. Define cumulative hazards $\Lambda_j(t) = \int_0^t \lambda_j(s)\,ds$ and $N_j(t) = \int_0^t \nu_j(s)\,ds$. On one probability space draw independent $E_A, E_F \sim \mathrm{Exp}(1)$ and set

$$\tau_{A,j} = \inf\{t : \Lambda_j(t) \geq E_A\}, \qquad \tau_{F,j} = \inf\{t : N_j(t) \geq E_F\}.$$

The order in (S7.1) gives $\tau_{A,2} \leq \tau_{A,1}$ and $\tau_{F,2} \geq \tau_{F,1}$ pathwise. If attention wins under system 1 by time t, then

$$\tau_{A,2} \leq \tau_{A,1} < \tau_{F,1} \leq \tau_{F,2},$$

so attention also wins under system 2 by t. Hence the attention-winning event under system 1 is a subset of that under system 2. Conversely, if fusion wins under system 2 by t, then

$$\tau_{F,1} \leq \tau_{F,2} < \tau_{A,2} \leq \tau_{A,1},$$

so fusion also wins under system 1. Taking probabilities yields (S7.2). $\square$

Proof of Generalized critical condition (technical-appendix result, S8.1)

Proof. Equation (S8.4) has two distinct positive roots exactly when its discriminant is positive. This gives (S8.5). The stability classification follows as in the baseline system: the lower root is a saddle and the upper root is locally asymptotically stable, while the origin remains locally asymptotically stable. At discriminant zero the two positive roots coalesce and the determinant of the Jacobian vanishes, giving the fold. □

Proof of Generalized watershed monotonicity (technical-appendix result, S8.2)

Proof. The discriminant in (S8.6) is strictly increasing in R_v, hence in ℓ. Differentiating the two root branches gives opposite signs. Because $v = d_q/[\rho(1-q)]$ is strictly increasing in q, the v branches inherit the same signs. □

Proof of Persistent-basin nesting under formation and retention learning (technical-appendix result, S8.3)

Proof. For the same initial condition, Appendix S6's first-contact argument applies to the two-dimensional post-withdrawal system: the larger-ℓ vector field is weakly larger in the v component and the system is cooperative. Hence trajectories under ℓ_2 dominate those under ℓ_1 componentwise. There are no periodic orbits in the positive interior: with Dulac function $B(q, v) = 1/q$,

$$\frac{\partial}{\partial q}(B\dot{q}) + \frac{\partial}{\partial v}(B\dot{v}) = -\rho v - a_v(\ell) - \frac{d_v(\ell)}{q} < 0.$$

The same Green's-theorem argument as in the basin-nesting proof above excludes closed graphics, so by the planar Poincaré–Bendixson theorem every omega-limit set in the square is a single equilibrium; an interior trajectory can therefore converge only to the origin, the saddle, or the positive attractor. By Corollary S8.2, increasing ℓ lowers the saddle and raises the positive attractor. A trajectory that converges to the positive attractor under ℓ_1 is componentwise dominated by the ℓ_2 trajectory and cannot converge to the lower origin or the lower saddle under ℓ_2. It must therefore converge to the positive attractor, proving (S8.7). □

Proof of Closed-form generalized critical legibility (technical-appendix result, S8.4)

Proof. Set $y = a_{v0} + a_{v1}\ell$. The threshold equation becomes

$$y \exp\left\{\frac{\omega_v}{a_{v1}} y\right\} = K \exp\left\{\frac{\omega_v a_{v0}}{a_{v1}}\right\}.$$

Multiplying by ω_v/a_{v1} and applying the defining identity $W(x)e^{W(x)} = x$ gives (S8.10). The zero-ω_v limit recovers the affine baseline by continuity. For monotonicity, define

$$F(\ell, \omega) = a_{v0} + a_{v1}\ell - Ke^{-\omega\ell}.$$

At the threshold, $F = 0$, while

$$F_\ell = a_{v1} + K\omega e^{-\omega\ell} > 0, \qquad F_\omega = K\ell e^{-\omega\ell} > 0$$

for $\ell > 0$. The implicit-function theorem therefore gives $d\ell^\dagger/d\omega = -F_\omega/F_\ell < 0$. □

Proof of Nonnegative direct effects preserve all entry orderings (technical-appendix result, S9.1)

Proof. For $\ell_2 > \ell_1$, the central structural path gives $\lambda_A(t;\ell_2) \geq \lambda_A(t;\ell_1)$. The multiplier $e^{\theta_\ell \ell}$ is also nondecreasing, so $\widetilde{\lambda}_A(t;\ell_2) \geq \widetilde{\lambda}_A(t;\ell_1)$. Every downstream ordering follows from the same cumulative-hazard and latent-clock arguments as before. □

Proof of Exact two-point condition with an adverse direct effect (technical-appendix result, S9.2)

Proof. Take the log of the ratio $\widetilde{\lambda}_A(t;\ell_2)/\widetilde{\lambda}_A(t;\ell_1)$. The common pressure path cancels, leaving exactly the left-hand side of (S9.3). The hazard ratio is at least one if and only if this log ratio is nonnegative. □

Proof of Continuous-time invariance and exact path solution (technical-appendix result, S10.1)

Proof. At $\ell = 0$, the right-hand side of (S10.1) is $\eta Y \geq 0$; at $\ell = 1$, it is $-(\delta_\ell + \chi G) \leq 0$, proving invariance. Equation (S10.1) is linear in ℓ; multiplication by the integrating factor $e^{K(t)}$ and integration yields (S10.3). □

Proof of Continuous-time environment comparison (technical-appendix result, S10.3)

Proof. At a common value $\ell \in [0,1]$, the difference between the two vector fields is

$$\eta\{Y_2 - Y_1\}(1-\ell) + \chi\{G_1 - G_2\}\ell \geq 0.$$

A scalar first-contact comparison therefore prevents the higher-opportunity/lower-capture path from crossing below the other path. □

S4 Nestedness check against the inherited entry model

Set A fixes $a_v = 1$ and suppresses the new $R/A/F$ hazards and inter-episode learning. Figure S1 reproduces three baseline objects: the inverted-U in early curiosity, the corresponding interior maximum of the early candidate-opening probability, and the post-withdrawal q–v phase portrait. Numerically, early curiosity peaks at $u \simeq 0.525$ and the early one-period candidate-opening probability peaks at $u \simeq 0.24$. The post-withdrawal equilibria are

$$(q_-, v_-) = (0.1333, 0.3077), \qquad (q_+, v_+) = (0.6000, 0.6667), \tag{S4.1}$$

which coincide with the preceding baseline.

The schedule-level recovery is shown in Table S1. In particular, the tapered schedule again reaches $(q,v) \simeq (0.600, 0.667)$ after the token has disappeared, with $g \simeq 0$, $\kappa \simeq 0.706$, a local candidate-opening probability near 0.639, and cumulative token spending 9.6. By contrast, the high fixed schedule produces cumulative candidate-opening probability about 0.502, below the no-reward level 0.699. These values are included solely to establish numerical nestedness.

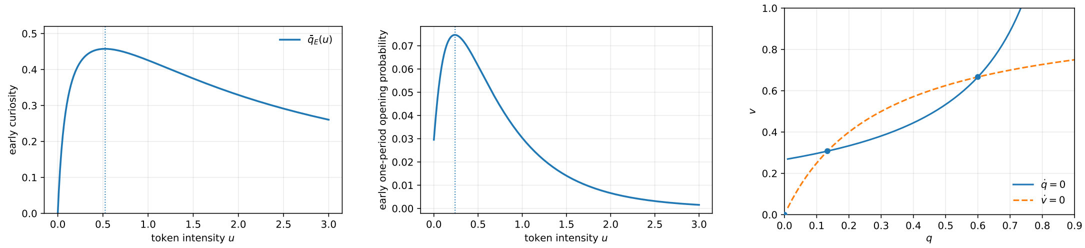

(a) Early curiosity.

(b) Early candidate opening.

(c) Post-withdrawal phase portrait.

Figure S1: Set A: numerical recovery of the preceding paper. The recovery is deliberately reported before any learning parameter is introduced.

Table S1: Set A: schedule recovery at $t = 40$

Schedule	q	v	g	κ	$p_1(40)$	$P(\tau_O \le 40)$	Spend
No reward	0.000	0.000	0.000	0.000	0.030	0.699	0.0
Moderate fixed	0.555	0.649	1.000	0.302	0.161	0.999	32.0
High fixed	0.385	0.562	2.500	0.106	0.016	0.502	80.0
Tapered	0.600	0.667	0.000	0.706	0.639	> 0.9999	9.6
Attention KPI	0.418	0.582	1.800	0.151	0.038	0.798	32.0

S5 Closed-loop simulation: implementation details and drift map

This section documents the Set E computation of the main text: the algorithm, the estimated experience curve $\mathbb{E}[Y \mid \ell]$, the induced effective drift, and the boundary of what the simulation shows.

S5.1 Algorithm

Within an episode the fast path is deterministic given ℓ, because the discrete state does not feed back into the continuous equations. Each episode is therefore simulated in two layers: a numerically integrated fast path, and, conditional on that path, an exact inversion of the jump clocks. First, the fast system is integrated once on $[0, T]$ with $T = 40$, $u = 0.8$, $z = 0$, and initial state $(0, 0, 0, 0)$, and the cumulative hazards $\Lambda_A(t) = \int_0^t \lambda_A$, $\Lambda_F(t) = \int_0^t \nu_F$, and $M_R(t) = \int_0^t \mu_R$, together with the cumulative qualified-exposure integrand $\int_0^t v\kappa$, are stored on a grid of step 0.02. Second, the three-state process is generated by inversion. From an R entry at time s, independent unit exponentials E_A, E_F are drawn; the candidate transition times are the first t with $\Lambda_A(t) - \Lambda_A(s) \ge E_A$ and with $\Lambda_F(t) - \Lambda_F(s) \ge E_F$; the earlier candidate wins; fusion is absorbing within the episode; and an attention entry at τ is followed by a re-closure time constructed from $M_R(t) - M_R(\tau)$ and a fresh exponential. After a re-closure the competition restarts from the re-closure time with fresh exponentials, which is the exact construction for a Markov jump process modulated by the (numerically integrated) deterministic path. The realized qualified exposure $\int \mathbf{1}_{\{S=A\}} v\kappa \, dt$ is accumulated over the A spells, Y_n and G_n follow from the canonical closures with $\omega_Y = 1.0$ and the stated ω_G, and ℓ_{n+1} follows from the slow map. Fast paths are precomputed on an ℓ grid of step 0.0025 covering the full state space $[0, 1]$ and looked up by nearest neighbor, so the induced error in $a_v(\ell)$ is at most 5×10^{-4}. The reported statistics use 4,000 replications of 60 episodes for each capture level and 20,000 episode simulations per grid point for the experience curve; all randomness derives from fixed seeds recorded in the reproduction script.

S5.2 The estimated experience curve and the effective drift

Because the pressure path is deterministic under constant inputs, G_n is constant and all endogenous randomness enters through Y_n. Figure S2(a) reports the Monte Carlo estimate of $\mathbb{E}[Y \mid \ell]$ together with the zero-drift requirement

$$Y_{\text{req}}(\ell) = \frac{(\delta_\ell + \chi G)\,\ell}{\eta\,(1-\ell)}, \tag{S5.1}$$

whose intersection with the experience curve is the mean-drift zero $\hat{\ell}$, the mean-field analogue of the slow target. Two features drive the main-text results. First, the curve is low and flat: a qualified A spell occurs in only 13–17% of episodes over $\ell \in [0, 0.35]$, with conditional exposure $\mathbb{E}[\int \mathbf{1}_{\{S=A\}} \upsilon\kappa\, dt \mid A]$ between 1.2 and 1.7, so $\mathbb{E}[Y \mid \ell]$ ranges only from 0.073 to about 0.11. The distribution of Y_n therefore mixes a large atom at zero (episodes resolved by fusion, or left unresolved, before any entry) with a jump of size roughly 0.7; realized slow paths are jump–decay sawtooths rather than smooth curves. Second, the intersection moves across $\ell^\dagger$ as the capture level changes: $\hat{\ell} = 0.268 > \ell^\dagger$ at $G = 0.033$, but $\hat{\ell} = 0.138 < \ell^\dagger$ at Set C's own level $G = 0.100$, with effective drift at the geometric threshold $\varphi(\ell^\dagger) = +0.002$ and -0.011 respectively (Figure S2(b)); Monte Carlo uncertainty for these quantities, a third capture level, and grid-convergence checks are reported in Section S5.3. The Set C benchmark value $\bar{Y} = 0.40$ is thus endogenously unattainable under these illustrative hazards; the loop sustains only $\bar{Y}_{\text{endog}} \approx 0.09$–$0.10$. Figure S3 shows sample paths at the Set C capture level: excursions above $\ell^\dagger$ occur through occasional qualified jumps but are almost always transient.

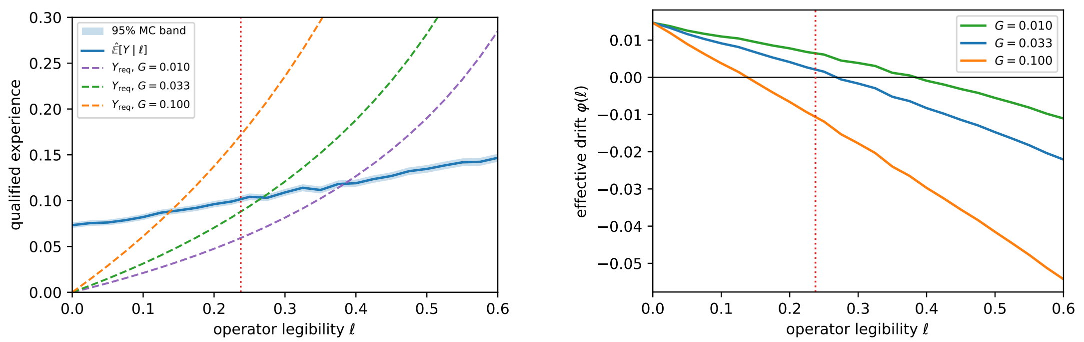

(a) Experience curve with pointwise 95% Monte Carlo band, and zero-drift requirements.

(b) Effective drift $\varphi(\ell)$ at three capture levels.

Figure S2: Closed-loop ingredients for Set E at capture levels $G \in \{0.010, 0.033, 0.100\}$. The dotted vertical line is $\ell^\dagger$; the shaded band in (a) is the pointwise 95% Monte Carlo interval, barely visible at 20,000 simulations per grid point.

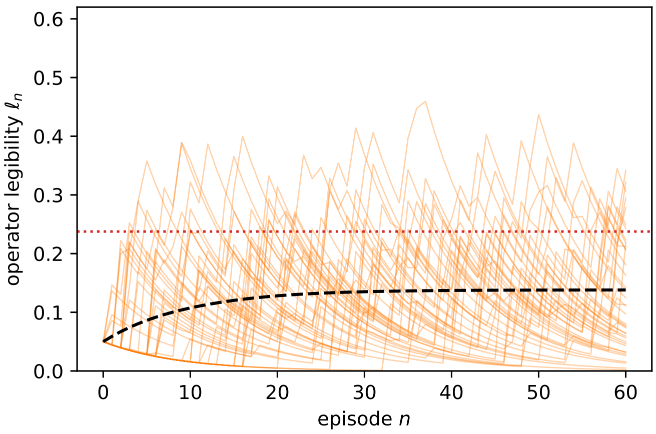

Figure S3: Set E sample paths at the Set C capture level $G = 0.100$. The dashed curve is the mean-field path computed from the estimated experience curve; the dotted line is $\ell^\dagger$.

S5.3 Monte Carlo uncertainty, regime classification, and numerical convergence

Three additions quantify the numerical reliability of the closed-loop statements.

Uncertainty at the geometric threshold. The drift sign at $\ell^\dagger$ decides the regime classification, so it is estimated directly rather than by grid interpolation: a dedicated fast path at $\ell = \ell^\dagger$ and 200,000 episode simulations give $\hat{\mathbb{E}}[Y \mid \ell^\dagger] = 0.0998$ (Monte Carlo standard error 0.0006), against 0.1016 from linear interpolation of the 0.025-grid curve; the interpolation gap (-0.0019) is of the same order as the per-point standard errors (0.0016–0.0022), which is why the direct evaluation is used. The implied drifts are $\varphi(\ell^\dagger) = +0.0062$, $+0.0018$, and -0.0109 at $G = 0.010$, 0.033, and 0.100, each with standard error 9×10^{-5}; the sign at the near-critical level $G = 0.033$ is therefore positive at roughly 20 standard errors, and the classification is not a numerical artifact. Propagating the per-point standard errors of the experience curve through the drift-zero functional (4,000 parametric-bootstrap draws) gives 95% intervals for the mean-drift zero $\hat{\ell}$ that exclude $\ell^\dagger = 0.2376$ at every capture level (Table S2). Figure S2(a) displays the pointwise 95% Monte Carlo band around the experience curve.

Three closed-loop regimes. Table S2 adds a milder capture level $G = 0.010$ ($\omega_G = 2.6 \times 10^{-4}$) to the two main-text levels. The three levels realize the robustly positive, near-critical positive, and negative regimes of the same closed loop, so Set E is a regime classification of the loop rather than a refutation of the Set C benchmark. Path dependence attenuates but does not vanish in the robust regime: 66% of crossing paths still fall back below $\ell^\dagger$ at least once, against 90% near criticality.

Grid convergence. Halving both discretizations—the hazard/exposure grid from 0.02 to 0.01 and the fast-path ℓ grid from 0.0025 to 0.00125—and regenerating the experience curve, the direct threshold evaluation, and the 4,000-replication loops leaves every headline quantity unchanged to within Monte Carlo resolution (Table S3): $\hat{\ell}$ moves by at most 10^{-4}, $\varphi(\ell^\dagger)$ by about 10^{-5}, and the largest shift in any reported proportion is 0.007, on the order of one Monte Carlo standard error at 4,000 replications.

Table S2: Three closed-loop regimes of the same episode loop. $\hat{\ell}$ is the drift zero with a 95% interval from propagating the experience-curve Monte Carlo error; $\varphi(\ell^\dagger)$ is evaluated directly at $\ell^\dagger$ (200,000 episodes; standard error 9×10^{-5}); crossing statistics use 4,000 replications of 60 episodes.

Regime	G	ω_G	$\hat{\ell}$ [95% CI]	$\varphi(\ell^\dagger)$	ever	at n=60	first [IQR]	fallback	share
Robustly positive	0.010	2.6×10^{-4}	0.384 [0.375, 0.390]	+0.0062	0.97	0.81	17 [9, 27]	0.66	0.54
Near-critical positive	0.033	8.7×10^{-4}	0.268 [0.264, 0.274]	+0.0018	0.95	0.55	18 [10, 29]	0.90	0.39
Negative (Set C level)	0.100	2.7×10^{-3}	0.138 [0.134, 0.142]	−0.0109	0.84	0.14	21 [11, 34]	0.98	0.12

"ever" = share of paths crossing $\ell^\dagger$ at least once by episode 60; "at n=60" = share above $\ell^\dagger$ at episode 60; "first [IQR]" = median and interquartile range of the first-crossing episode among crossing paths; "fallback" = share of crossing paths that later fall back below $\ell^\dagger$; "share" = average share of episodes spent above $\ell^\dagger$.

All quantities in this subsection are regenerated by `run_set_E_uncertainty()` in the reproduction script and written to `setE_uncertainty.csv`, `setE_regimes.csv`, and `setE_convergence.csv`.

Table S3: Grid-convergence check. Both discretizations are halved with identical seeds; M = 20,000 per curve point, 200,000 at $\ell^\dagger$, 4,000 replications per loop.

Quantity	Baseline	Halved	|difference|
$\hat{\mathbb{E}}[Y \mid \ell^\dagger]$ (direct)	0.09975	0.09979	0.00004
$\varphi(\ell^\dagger)$, $G = 0.033$	+0.00181	+0.00182	0.00001
$\varphi(\ell^\dagger)$, $G = 0.100$	−0.01093	−0.01092	0.00001
$\hat{\ell}$, $G = 0.033$	0.2683	0.2683	$< 10^{-4}$
$\hat{\ell}$, $G = 0.100$	0.1381	0.1380	0.0001
share above at n=60, $G = 0.033$	0.554	0.553	0.001
share above at n=60, $G = 0.100$	0.139	0.146	0.007
share of episodes above, $G = 0.033$	0.388	0.388	0.001
share of episodes above, $G = 0.100$	0.1218	0.1217	0.0001
$\max_\ell \lvert\Delta\hat{\mathbb{E}}[Y \mid \ell]\rvert$ over the grid	—	—	0.0003

S5.4 What the simulation does and does not show

The simulation displays a regime of the closed loop; it proves nothing beyond the theorems already stated. In particular, no monotonicity of $\mathbb{E}[Y \mid \ell]$ is claimed: the estimated curve is increasing, but the matched-state boundary discussed in the main text blocks a pathwise proof, and other closure constants place the loop in monotone-collapse or comfortable-climb regimes in which the displayed path dependence is muted (Table S2 realizes the mild-capture case explicitly). What the simulation adds to the analytical results is a caution and a phenomenon. The caution is that constant-summary benchmarks can overstate what the loop endogenously sustains, so a positive exogenous persistence margin does not guarantee a positive endogenous one. The phenomenon is punctuated learning with intermittent persistence windows, in which whether a given history is above the geometric threshold at a given episode is substantially decided by the arrival pattern of rare qualified episodes.

S6 Fast-system invariance and comparison in full detail

S6.1 A generalized within-episode system

For this appendix, write the fast system as

$$\dot{q} = a_q\mathcal{E}(u)(1-q) + \rho v q(1-q) - \{d_q + b_q g\}q, \tag{S6.1}$$

$$\dot{v} = a_v(\ell)q(1-v) - d_v(\ell)v, \tag{S6.2}$$

$$\dot{g} = a_g u + a_z z - d_g g, \tag{S6.3}$$

$$\dot{\kappa} = a_\kappa q v(1-\kappa) - \{d_\kappa + b_\kappa g\}\kappa. \tag{S6.4}$$

The central specification in the main text has constant d_v and affine $a_v(\ell)$. Here we only require

$$a_v(\ell) > 0, \qquad a_v'(\ell) \geq 0, \qquad d_v(\ell) > 0, \qquad d_v'(\ell) \leq 0. \tag{S6.5}$$

Thus greater legibility may improve current visibility either by raising formation efficiency, by lowering visibility decay, or by both channels.

Lemma S6.1 (Positive invariance of the fast state space). *If $u, z \geq 0$, $q(0), v(0), \kappa(0) \in [0,1]$, and $g(0) \geq 0$, then the solution of* (S6.1)–(S6.4) *satisfies*

$$q(t), v(t), \kappa(t) \in [0,1], \qquad g(t) \geq 0$$

for every time at which the solution exists.

Proof. The vector field points inward on every boundary face. At $q = 0$, $\dot{q} = a_q\mathcal{E}(u) \geq 0$; at $q = 1$, $\dot{q} = -(d_q + b_q g) \leq 0$. At $v = 0$, $\dot{v} = a_v(\ell)q \geq 0$; at $v = 1$, $\dot{v} = -d_v(\ell) \leq 0$. At $\kappa = 0$, $\dot{\kappa} = a_\kappa q v \geq 0$; at $\kappa = 1$, $\dot{\kappa} = -(d_\kappa + b_\kappa g) \leq 0$. Finally, at $g = 0$, $\dot{g} = a_g u + a_z z \geq 0$. A first-exit argument therefore rules out departure from the stated domain. □

Lemma S6.2 (Generalized matched-path comparison). *Let $0 \leq \ell_1 < \ell_2 \leq 1$. Compare two episodes with identical bounded input paths $u(t), z(t)$ and identical initial fast states. Under* (S6.5)*,*

$$q(t;\ell_2) \geq q(t;\ell_1), \quad v(t;\ell_2) \geq v(t;\ell_1), \quad \kappa(t;\ell_2) \geq \kappa(t;\ell_1) \tag{S6.6}$$

for all $t \geq 0$, while $g(t;\ell_2) = g(t;\ell_1)$.

Proof. The pressure equation (S6.3) is independent of ℓ, q, v, κ, so the two g paths coincide. Fix this common path and let $x = (q, v, \kappa)$. The subsystem is cooperative because its off-diagonal derivatives are

$$\frac{\partial \dot{q}}{\partial v} = \rho q(1-q) \geq 0, \qquad \frac{\partial \dot{v}}{\partial q} = a_v(\ell)(1-v) \geq 0,$$

$$\frac{\partial \dot{\kappa}}{\partial q} = a_\kappa v(1-\kappa) \geq 0, \qquad \frac{\partial \dot{\kappa}}{\partial v} = a_\kappa q(1-\kappa) \geq 0.$$

At a common state x, only the v component changes directly with ℓ, and

$$\dot{v}(x;\ell_2) - \dot{v}(x;\ell_1) = \{a_v(\ell_2) - a_v(\ell_1)\}q(1-v) \tag{S6.7}$$

$$+ \{d_v(\ell_1) - d_v(\ell_2)\}v \geq 0. \tag{S6.8}$$

Suppose that the componentwise order first failed at time t^*. At the first contact of the difference process with a boundary of the nonnegative cone, the derivative of the zero component cannot point outward: if $q_2 = q_1$, its derivative difference is $\rho q(1-q)(v_2 - v_1) \geq 0$; if $v_2 = v_1$, the derivative difference is nonnegative by (S6.8) together with $q_2 \geq q_1$; and if $\kappa_2 = \kappa_1$, its derivative difference is nonnegative because the κ vector field is increasing in both q and v. Hence no first outward crossing exists, proving (S6.6). □

Remark S6.3 (What the generalized comparison buys). *The baseline proof used only $a_v'(\ell) \geq 0$. Lemma S6.2 shows that the transition ordering is strengthened, not weakened, if repeated qualified experience also makes newly visible structure fade more slowly, provided $d_v'(\ell) \leq 0$. The central paper therefore uses the more conservative one-channel specification.*

S7 Time-varying competing risks: a general ordering theorem

The main text uses two first-exit intensities from the unresolved state R: attention entry $\lambda_A(t;\ell)$ and fusion $\nu_F(t;\ell)$. The following result is stated directly for arbitrary locally integrable hazards and does not use the particular exponential specification.

Theorem S7.1 (Monotone competing-risks coupling). *Let $(\lambda_j(t), \nu_j(t))$, $j = 1, 2$, be nonnegative locally integrable cause-specific hazards satisfying*

$$\lambda_2(t) \geq \lambda_1(t), \qquad \nu_2(t) \leq \nu_1(t) \quad \text{for almost every } t \geq 0. \tag{S7.1}$$

Let $C_{A,j}(t)$ and $C_{F,j}(t)$ denote the cumulative incidences that attention and fusion, respectively, are the first exit from R by horizon t. Then

$$C_{A,2}(t) \geq C_{A,1}(t), \qquad C_{F,2}(t) \leq C_{F,1}(t) \quad (t \geq 0). \tag{S7.2}$$

Proof. Define cumulative hazards $\Lambda_j(t) = \int_0^t \lambda_j(s)\,ds$ and $N_j(t) = \int_0^t \nu_j(s)\,ds$. On one probability space draw independent $E_A, E_F \sim \mathrm{Exp}(1)$ and set

$$\tau_{A,j} = \inf\{t : \Lambda_j(t) \geq E_A\}, \qquad \tau_{F,j} = \inf\{t : N_j(t) \geq E_F\}.$$

The order in (S7.1) gives $\tau_{A,2} \leq \tau_{A,1}$ and $\tau_{F,2} \geq \tau_{F,1}$ pathwise. If attention wins under system 1 by time t, then

$$\tau_{A,2} \leq \tau_{A,1} < \tau_{F,1} \leq \tau_{F,2},$$

so attention also wins under system 2 by t. Hence the attention-winning event under system 1 is a subset of that under system 2. Conversely, if fusion wins under system 2 by t, then

$$\tau_{F,1} \leq \tau_{F,2} < \tau_{A,2} \leq \tau_{A,1},$$

so fusion also wins under system 1. Taking probabilities yields (S7.2). □

Corollary S7.2 (Application to operator legibility). *Under the matched-path comparison of Appendix S6, suppose $\pi(\kappa)$ is nondecreasing, the entry intensity is nondecreasing in q, v, κ, and the fusion intensity is nonincreasing in v, κ, ℓ. Then $\ell_2 > \ell_1$ implies the cumulative-incidence ordering* (S7.2).

Remark S7.3 (No theorem for total resolution time)**.** *The theorem deliberately orders the* composition *of first exits, not the time to whichever exit occurs first. The total hazard is $\lambda_j + \nu_j$; one component rises while the other falls, so the total need not be ordered. This is a useful falsifiability boundary: the model predicts earlier cause-specific attention entry and less fusion, not necessarily shorter unresolved spells of every kind.*

S7.1 Matched-state re-closure as a one-risk special case

If $\mu_2(t) \le \mu_1(t)$ are the first re-closure hazards from a matched A state, then

$$\Pr\{T_{R,2} > H\} = \exp\left\{-\int_0^H \mu_2(s)\,ds\right\} \ge \exp\left\{-\int_0^H \mu_1(s)\,ds\right\} = \Pr\{T_{R,1} > H\}.$$

Thus the re-closure result is the single-risk counterpart of Theorem S7.1. An unconditional comparison beginning at each ℓ-specific endogenous entry state remains outside the claim because the starting state itself is then selected by the earlier competing-risk process.

S8 Robustness to legibility-dependent visibility retention

S8.1 The effective visibility ratio

After withdrawal, set $u = z = g = 0$ and consider

$$\dot{q} = q\{\rho v(1-q) - d_q\}, \tag{S8.1}$$
$$\dot{v} = a_v(\ell)q(1-v) - d_v(\ell)v. \tag{S8.2}$$

Define the effective visibility ratio

$$R_v(\ell) := \frac{a_v(\ell)}{d_v(\ell)}. \tag{S8.3}$$

The q-nullcline is $v = d_q/[\rho(1-q)]$, while the v-nullcline is

$$v = \frac{R_v(\ell)q}{1 + R_v(\ell)q}.$$

Their positive intersections solve

$$\rho q^2 - (\rho - d_q)q + \frac{d_q}{R_v(\ell)} = 0. \tag{S8.4}$$

Proposition S8.1 (Generalized critical condition)**.** *Assume $\rho > d_q$. Positive saddle–attractor pairs exist if and only if*

$$R_v(\ell) > R_v^* := \frac{4\rho d_q}{(\rho - d_q)^2}. \tag{S8.5}$$

At equality there is a nonhyperbolic fold, and below equality the origin is the only *equilibrium in the nonnegative state space. When* (S8.5) *holds,*

$$q_\pm(\ell) = \frac{(\rho - d_q) \pm \sqrt{(\rho - d_q)^2 - 4\rho d_q/R_v(\ell)}}{2\rho}, \tag{S8.6}$$

with $v_\pm = d_q/[\rho(1 - q_\pm)]$.

Proof. Equation (S8.4) has two distinct positive roots exactly when its discriminant is positive. This gives (S8.5). The stability classification follows as in the baseline system: the lower root is a saddle and the upper root is locally asymptotically stable, while the origin remains locally asymptotically stable. At discriminant zero the two positive roots coalesce and the determinant of the Jacobian vanishes, giving the fold. ☐

Corollary S8.2 (Generalized watershed monotonicity)**.** *If* $R_v'(\ell) > 0$ *throughout a bistable interval, then*

$$q_-'(\ell) < 0 < q_+'(\ell), \qquad v_-'(\ell) < 0 < v_+'(\ell).$$

Thus the saddle moves southwest and the positive attractor northeast whenever experience raises the formation-to-decay ratio of current visibility.

Proof. The discriminant in (S8.6) is strictly increasing in R_v, hence in ℓ. Differentiating the two root branches gives opposite signs. Because $v = d_q/[\rho(1 - q)]$ is strictly increasing in q, the v branches inherit the same signs. ☐

Theorem S8.3 (Persistent-basin nesting under formation and retention learning)**.** *Suppose* $\ell_2 > \ell_1$ *are both in the bistable region,* $a_v(\ell_2) \geq a_v(\ell_1)$*, and* $d_v(\ell_2) \leq d_v(\ell_1)$*. Let* $\mathcal{B}_+(\ell)$ *be the basin of the positive stable equilibrium in* $(0, 1)^2$*. Then*

$$\mathcal{B}_+(\ell_1) \subseteq \mathcal{B}_+(\ell_2). \tag{S8.7}$$

Proof. For the same initial condition, Appendix S6's first-contact argument applies to the two-dimensional post-withdrawal system: the larger-ℓ vector field is weakly larger in the v component and the system is cooperative. Hence trajectories under ℓ_2 dominate those under ℓ_1 componentwise. There are no periodic orbits in the positive interior: with Dulac function $B(q, v) = 1/q$,

$$\frac{\partial}{\partial q}(B\dot{q}) + \frac{\partial}{\partial v}(B\dot{v}) = -\rho v - a_v(\ell) - \frac{d_v(\ell)}{q} < 0.$$

The same Green's-theorem argument as in the basin-nesting proof above excludes closed graphics, so by the planar Poincaré–Bendixson theorem every omega-limit set in the square is a single equilibrium; an interior trajectory can therefore converge only to the origin, the saddle, or the positive attractor. By Corollary S8.2, increasing ℓ lowers the saddle and raises the positive attractor. A trajectory that converges to the positive attractor under ℓ_1 is componentwise dominated by the ℓ_2 trajectory and cannot converge to the lower origin or the lower saddle under ℓ_2. It must therefore converge to the positive attractor, proving (S8.7). ☐

S8.2 An explicit affine–exponential specification

A convenient two-channel robustness specification is

$$a_v(\ell) = a_{v0} + a_{v1}\ell, \qquad d_v(\ell) = d_{v0}e^{-\omega_v \ell}, \qquad a_{v1} > 0,\ \omega_v \geq 0. \tag{S8.8}$$

Let

$$K := d_{v0}R_v^* = \frac{4\rho d_q d_{v0}}{(\rho - d_q)^2}. \tag{S8.9}$$

The critical condition is $a_{v0} + a_{v1}\ell = Ke^{-\omega_v \ell}$.

Proposition S8.4 (Closed-form generalized critical legibility)**.** *Under* (S8.8)*, if* $\omega_v > 0$ *and the critical point lies in* $[0, 1]$*, it is*

$$\ell^\dagger_\omega = \frac{1}{\omega_v} W_0\left(\frac{\omega_v K}{a_{v1}} \exp\left\{\frac{\omega_v a_{v0}}{a_{v1}}\right\}\right) - \frac{a_{v0}}{a_{v1}}, \tag{S8.10}$$

where W_0 *is the principal real Lambert* W *branch (Corless et al., 1996). As* $\omega_v \downarrow 0$*,* (S8.10) *converges to the baseline threshold* $(K - a_{v0})/a_{v1}$*. Whenever* $\ell^\dagger_\omega > 0$*,*

$$\frac{\partial \ell^\dagger_\omega}{\partial \omega_v} < 0. \tag{S8.11}$$

Proof. Set $y = a_{v0} + a_{v1}\ell$. The threshold equation becomes

$$y \exp\left\{\frac{\omega_v}{a_{v1}} y\right\} = K \exp\left\{\frac{\omega_v a_{v0}}{a_{v1}}\right\}.$$

Multiplying by ω_v/a_{v1} and applying the defining identity $W(x)e^{W(x)} = x$ gives (S8.10). The zero-ω_v limit recovers the affine baseline by continuity. For monotonicity, define

$$F(\ell, \omega) = a_{v0} + a_{v1}\ell - Ke^{-\omega \ell}.$$

At the threshold, $F = 0$, while

$$F_\ell = a_{v1} + K\omega e^{-\omega\ell} > 0, \qquad F_\omega = K\ell e^{-\omega \ell} > 0$$

for $\ell > 0$. The implicit-function theorem therefore gives $d\ell^\dagger/d\omega = -F_\omega/F_\ell < 0$. ☐

S9 Robustness to a direct legibility term in the entry hazard

The central specification intentionally keeps ℓ out of the attention-entry hazard and lets the effect operate through $a_v(\ell)$ and the fast path. This is the conservative formulation because it prevents the main result from being a restatement of a direct positive coefficient. Suppose instead that the model is augmented by

$$\widetilde{\lambda}_A(t; \ell) = \lambda_A(t; \ell) \exp\{\theta_\ell \ell\}, \tag{S9.1}$$

where λ_A is the central structural-path intensity.

Proposition S9.1 (Nonnegative direct effects preserve all entry orderings)**.** *If* $\theta_\ell \geq 0$*, then every pointwise, cumulative-hazard, first-order stochastic-dominance, and* *competing-incidence ordering for attention entry established under the central specification remains valid under* (S9.1)*.*

Proof. For $\ell_2 > \ell_1$, the central structural path gives $\lambda_A(t;\ell_2) \geq \lambda_A(t;\ell_1)$. The multiplier $e^{\theta_\ell \ell}$ is also nondecreasing, so $\widetilde{\lambda}_A(t;\ell_2) \geq \widetilde{\lambda}_A(t;\ell_1)$. Every downstream ordering follows from the same cumulative-hazard and latent-clock arguments as before. □

Proposition S9.2 (Exact two-point condition with an adverse direct effect)**.** *Assume* $\pi(\kappa(t;\ell_j)) > 0$ *for* $j = 1, 2$*. Let* $\Delta x = x(t;\ell_2) - x(t;\ell_1)$ *and* $\Delta\ell = \ell_2 - \ell_1 > 0$*. Then*

$$\widetilde{\lambda}_A(t;\ell_2) \geq \widetilde{\lambda}_A(t;\ell_1) \tag{S9.2}$$

if and only if

$$\theta_q \Delta q + \theta_v \Delta v + \theta_\kappa \Delta\kappa + \log \frac{\pi(\kappa(t;\ell_2))}{\pi(\kappa(t;\ell_1))} + \theta_\ell \Delta\ell \geq 0. \tag{S9.3}$$

Hence a modest negative direct coefficient $\theta_\ell < 0$ *need not overturn the main result if the indirect structural gain is sufficiently large.*

Proof. Take the log of the ratio $\widetilde{\lambda}_A(t;\ell_2)/\widetilde{\lambda}_A(t;\ell_1)$. The common pressure path cancels, leaving exactly the left-hand side of (S9.3). The hazard ratio is at least one if and only if this log ratio is nonnegative. □

Corollary S9.3 (Optional direct legibility terms are unnecessary for fusion and re-closure)**.** *The central fusion and re-closure hazards contain no direct* ℓ *loading. If they are augmented by multiplicative factors* $\exp\{-\phi_\ell \ell\}$ *and* $\exp\{-\psi_\ell \ell\}$ *with nonnegative coefficients, the established hazard orderings are only strengthened. Setting these optional coefficients to zero recovers the central model, in which the orderings arise entirely through the matched-state improvement of* v *and* κ*.*

Remark S9.4 (Interpretation)**.** *The direct-effect robustness check clarifies rather than weakens the baseline design. Optional direct loadings are deliberately excluded from the central model. A nonnegative direct* θ_ℓ *only strengthens the entry result; a negative direct term creates a transparent dominance condition. The paper's central specification sets* $\theta_\ell = 0$ *so that the strongest result is obtained without assuming that legibility itself mechanically raises attention entry.*

S10 Continuous-time learning and the discrete-map limit

The main text uses episode time because qualified experience is summarized once per episode. The same mechanism can be written in continuous slow time as

$$\dot{\ell}(t) = \eta Y(t)\{1 - \ell(t)\} - \{\delta_\ell + \chi G(t)\}\ell(t), \tag{S10.1}$$

where $Y(t), G(t) \in [0,1]$ are slow-time summaries.

Proposition S10.1 (Continuous-time invariance and exact path solution)**.** *If* $\ell(0) \in [0,1]$ *and* $Y, G \in [0,1]$*, then* $\ell(t) \in [0,1]$ *for all* $t \geq 0$*. Let*

$$K(t) = \int_0^t \{\eta Y(s) + \delta_\ell + \chi G(s)\}\, ds. \tag{S10.2}$$

Then

$$\ell(t) = e^{-K(t)} \left[\ell(0) + \int_0^t \eta Y(s) e^{K(s)}\, ds \right]. \tag{S10.3}$$

Proof. At $\ell = 0$, the right-hand side of (S10.1) is $\eta Y \geq 0$; at $\ell = 1$, it is $-(\delta_\ell + \chi G) \leq 0$, proving invariance. Equation (S10.1) is linear in ℓ; multiplication by the integrating factor $e^{K(t)}$ and integration yields (S10.3). □

Corollary S10.2 (Constant environment, threshold time, and persistence birth)**.** *If $Y(t) \equiv \bar{Y}$ and $G(t) \equiv \bar{G}$, define*

$$k = \eta \bar{Y} + \delta_\ell + \chi \bar{G}, \qquad \ell^* = \frac{\eta \bar{Y}}{k}.$$

Then

$$\ell(t) = \ell^* + \{\ell(0) - \ell^*\} e^{-kt}. \tag{S10.4}$$

If $\ell(0) < h < \ell^*$, the first continuous slow time at which ℓ reaches h is

$$t_h = \frac{1}{k} \log \frac{\ell^* - \ell(0)}{\ell^* - h}. \tag{S10.5}$$

Setting $h = \ell^\dagger$ gives the continuous-time birth time of persistence geometry whenever $\ell(0) < \ell^\dagger < \ell^*$.

Proposition S10.3 (Continuous-time environment comparison)**.** *Consider two slow environments with the same initial $\ell(0)$ and with $Y_2(t) \geq Y_1(t)$ and $G_2(t) \leq G_1(t)$ for all t. Then $\ell_2(t) \geq \ell_1(t)$ for all $t \geq 0$.*

Proof. At a common value $\ell \in [0, 1]$, the difference between the two vector fields is

$$\eta\{Y_2 - Y_1\}(1 - \ell) + \chi\{G_1 - G_2\}\ell \geq 0.$$

A scalar first-contact comparison therefore prevents the higher-opportunity/lower-capture path from crossing below the other path. □

S10.1 Relation to the discrete episode map

For a slow-time step $\Delta > 0$, forward Euler applied to (S10.1) gives

$$\ell_{n+1} = \ell_n + \Delta \left[\eta Y_n (1 - \ell_n) - \{\delta_\ell + \chi G_n\} \ell_n \right]. \tag{S10.6}$$

The main text normalizes $\Delta = 1$ and imposes the episode-wise monotone-range condition $\eta Y_n + \delta_\ell + \chi G_n \leq 1$ on the Euler coefficient; the primitive bound

$$\eta + \delta_\ell + \chi \leq 1$$

is the uniform-in-(Y, G) sufficient version of the same requirement and is not needed for the illustrations. The continuous-time law itself needs no such discretization restriction. Thus the restriction in Section 4 is a transparent episode-aggregation condition, not a substantive claim that the underlying learning process must be slow in an absolute physical-time sense.

S11 Sensitivity maps and additional phase portraits

This appendix uses the same near-critical primitives as the numerical section whenever possible: $\rho = 1.5$, $d_q = 0.4$, $d_{v0} = 0.3$, and $a_{v0} = 0.50$. No number below is a calibration. The figures show how the analytical thresholds move when robustness parameters are varied.

S11.1 How visibility retention lowers the critical legibility

Figure S4 plots the generalized threshold from Proposition S8.4. Increasing ω_v makes current structural visibility decay more slowly at higher legibility and therefore lowers the amount of legibility required to create the positive saddle–attractor pair. A larger formation-learning slope a_{v1} has the same directional effect.

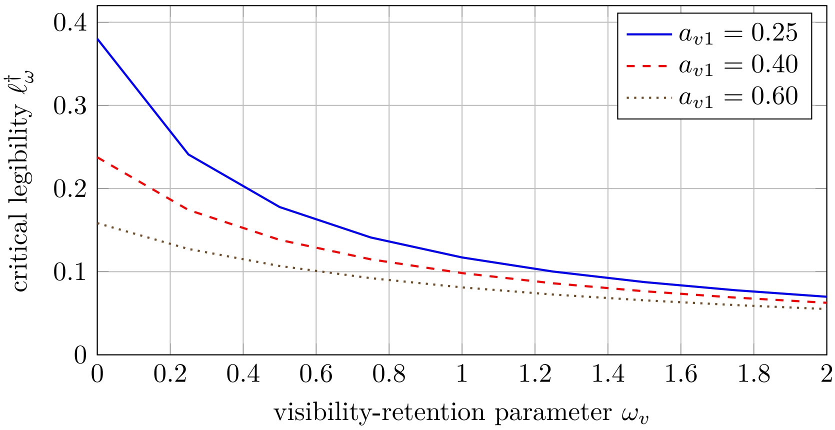

Figure S4: Generalized critical legibility under $a_v(\ell) = 0.50 + a_{v1}\ell$ and $d_v(\ell) = 0.30e^{-\omega_v \ell}$. The original near-critical case is the dashed curve at $\omega_v = 0$, where $\ell^\dagger \simeq 0.2376$.

S11.2 The persistence-learning boundary in experience–evaluation space

For a fixed critical level $\ell^\dagger$, the slow fixed point lies above the threshold exactly when

$$\eta \bar{Y}(1 - \ell^\dagger) > (\delta_\ell + \chi \bar{G})\ell^\dagger.$$

Using the near-critical values $\eta = 0.20$, $\delta_\ell = 0.03$, $\chi = 0.80$, and $\ell^\dagger = 0.2376$, the boundary is approximately

$$\bar{G}_{\text{crit}}(\bar{Y}) = 0.8022\bar{Y} - 0.0375.$$

Figure S5 makes the asymmetry visible: more qualified experience raises the evaluative pressure the system can tolerate, but high pressure can still place the long-run slow state below the geometric threshold.

S11.3 Additional phase portraits with formation and retention learning

Set $a_v(\ell) = 0.50 + 0.40\ell$ and $d_v(\ell) = 0.30e^{-0.75\ell}$. Proposition S8.4 gives $\ell^\dagger_\omega \simeq 0.1148$. Figure S6 shows three snapshots. At $\ell = 0.05$ no positive pair exists. Just above the

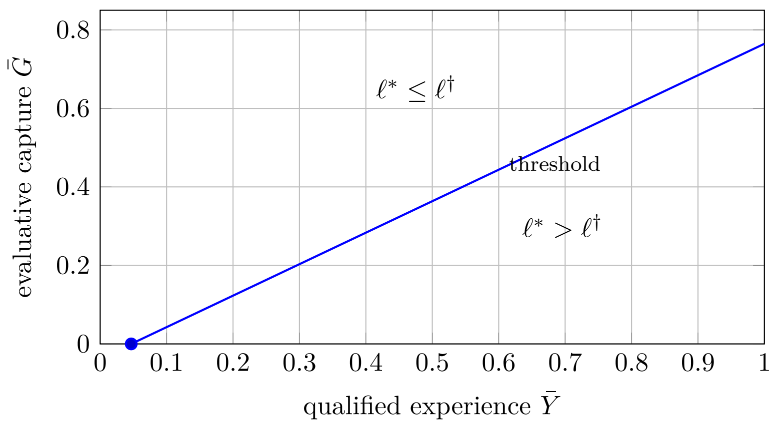

Figure S5: Persistence-learning boundary for the near-critical numerical primitives. The region below the line supports a slow fixed point above $\ell^\dagger$; the region above it does not.

threshold, at $\ell = 0.12$, the saddle and positive attractor are close. By $\ell = 0.50$ the saddle has moved substantially toward the origin and the upper attractor outward.

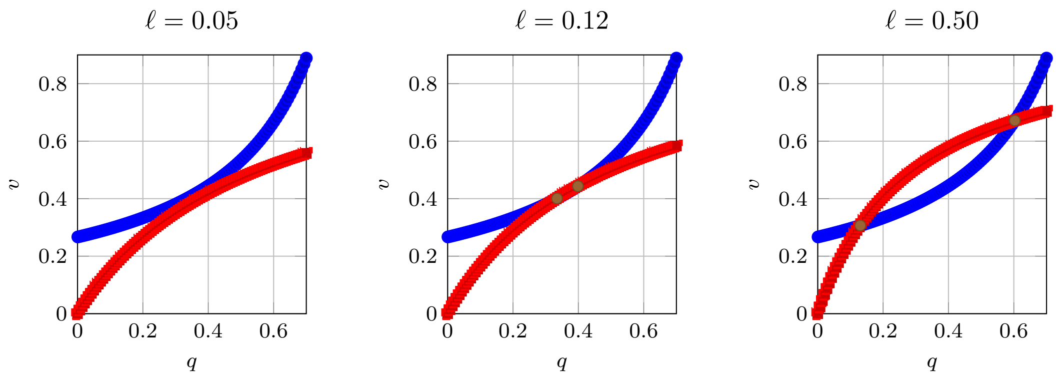

(a) Below threshold. (b) Just above threshold. (c) Expanded geometry.

Figure S6: Additional post-withdrawal phase portraits under both visibility-formation and visibility-retention learning. Solid: q-nullcline. Dashed: v-nullcline. Dots mark the positive saddle and attractor when they exist.

S12 Robustness ledger and scope

Robustness summary. The robustness layer establishes six statements simultaneously, without changing the central model: (i) the fast-path comparison has a self-contained proof; (ii) the competing-risk result holds for time-varying hazards, not only local constant approximations; (iii) the geometric threshold survives when legibility affects visibility retention as well as formation; (iv) direct hazard effects are shown to be optional rather than necessary; (v) the discrete slow map has a continuous-time counterpart with the same fixed point and threshold logic; and (vi) the numerical sensitivity figures illustrate, rather than create, the analytical conclusions.

Table S4: Which central results survive the robustness checks?

Modification	Required condition	Preserved conclusion
Legibility-dependent d_v	$a_v' \geq 0$, $d_v' \leq 0$	Fast-state order, lower watershed, basin nesting; threshold depends on a_v/d_v
Direct $\theta_\ell \ell$ in entry hazard	$\theta_\ell \geq 0$	All entry and competing-incidence orderings strengthen
Adverse direct entry term	Inequality (S9.3)	Entry ordering survives when structural gain dominates direct penalty
Optional direct ϕ_ℓ, ψ_ℓ set to zero	At least one indirect loading on v or κ	Fusion and re-closure can still improve entirely through the fast path
Continuous-time slow state	Same formation, loss, and capture signs	Same ℓ^*, positive/reverse learning split, exact threshold crossing, persistence birth
General time-varying hazards	Pointwise $\lambda_2 \geq \lambda_1$, $\nu_2 \leq \nu_1$	Attention cumulative incidence rises and fusion cumulative incidence falls

Resulting model boundary. The robustness layer does not turn the paper into a theory of trained attention. Across all specifications, the slow object remains operator legibility: a history-dependent condition that changes how recurrent self-referential structure becomes visible and, through that change, alters the subsequent transition law and persistence geometry. The model still permits flat and reverse learning, does not guarantee a first opening, and does not claim that repeated practice manufactures functional non-closure.

References

Andersen, P. K., and R. D. Gill. 1982. "Cox's Regression Model for Counting Processes: A Large Sample Study." *The Annals of Statistics* 10(4): 1100–1120. doi:10.1214/aos/1176345976.

Bernstein, A., Y. Hadash, Y. Lichtash, G. Tanay, K. Shepherd, and D. M. Fresco. 2015. "Decentering and Related Constructs: A Critical Review and Metacognitive Processes Model." *Perspectives on Psychological Science* 10(5): 599–617. doi:10.1177/1745691615594577.

Bolderston, H., D. T. Gillanders, G. Turner, H. C. Taylor, D. Ni Mhaoileoin, and A. Coleman. 2019. "The Initial Validation of a State Version of the Cognitive Fusion Questionnaire." *Journal of Contextual Behavioral Science* 12: 207–215. doi:10.1016/j.jcbs.2018.04.002.

Corless, R. M., G. H. Gonnet, D. E. G. Hare, D. J. Jeffrey, and D. E. Knuth. 1996. "On the Lambert W Function." *Advances in Computational Mathematics* 5(1): 329–359. doi:10.1007/BF02124750.

Cramer, A. O. J., C. D. van Borkulo, E. J. Giltay, H. L. J. van der Maas, K. S. Kendler, M. Scheffer, and D. Borsboom. 2016. "Major Depression as a Complex Dynamic System." *PLOS ONE* 11(12): e0167490. doi:10.1371/journal.pone.0167490.

Davis, M. H. A. 1984. "Piecewise-Deterministic Markov Processes: A General Class of Non-Diffusion Stochastic Models." *Journal of the Royal Statistical Society: Series B* 46(3): 353–388. doi:10.1111/j.2517-6161.1984.tb01308.x.

Gillanders, D. T., H. Bolderston, F. W. Bond, M. Dempster, P. E. Flaxman, L. Campbell, S. Kerr, et al. 2014. "The Development and Initial Validation of the Cognitive Fusion Questionnaire." *Behavior Therapy* 45(1): 83–101. doi:10.1016/j.beth.2013.09.001.

Goldstone, R. L. 1998. "Perceptual Learning." *Annual Review of Psychology* 49: 585–612. doi:10.1146/annurev.psych.49.1.585.

Groves, P. M., and R. F. Thompson. 1970. "Habituation: A Dual-Process Theory." *Psychological Review* 77(5): 419–450. doi:10.1037/h0029810.

Haslbeck, J. M. B., O. Ryan, D. J. Robinaugh, L. J. Waldorp, and D. Borsboom. 2022. "Modeling Psychopathology: From Data Models to Formal Theories." *Psychological Methods* 27(6): 930–957. doi:10.1037/met0000303.

Hougaard, P. 1999. "Multi-State Models: A Review." *Lifetime Data Analysis* 5(3): 239–264. doi:10.1023/A:1009672031531.

Kuehn, C. 2015. *Multiple Time Scale Dynamics.* Applied Mathematical Sciences 191. Cham: Springer. doi:10.1007/978-3-319-12316-5.

Lally, P., C. H. M. van Jaarsveld, H. W. W. Potts, and J. Wardle. 2010. "How Are Habits Formed: Modelling Habit Formation in the Real World." *European Journal of Social Psychology* 40(6): 998–1009. doi:10.1002/ejsp.674.

Laukkonen, R. E., and H. A. Slagter. 2021. "From Many to (n)one: Meditation and the Plasticity of the Predictive Mind." *Neuroscience & Biobehavioral Reviews* 128: 199–217. doi:10.1016/j.neubiorev.2021.06.021.

Lutz, A., A. P. Jha, J. D. Dunne, and C. D. Saron. 2015. "Investigating the Phenomenological Matrix of Mindfulness-Related Practices from a Neurocognitive Perspective." *American Psychologist* 70(7): 632–658. doi:10.1037/a0039585.

Oyama, H., T. Matsumoto, and J. Tani. 2025. "Modeling Autonomous Shifts between Focus State and Mind-Wandering Using a Predictive-Coding-Inspired Variational Recurrent Neural Network." *Frontiers in Computational Neuroscience* 19: 1578135. doi:10.3389/fncom.2025.1578135.

Putter, H., M. Fiocco, and R. B. Geskus. 2007. "Tutorial in Biostatistics: Competing Risks and Multi-State Models." *Statistics in Medicine* 26(11): 2389–2430. doi:10.1002/sim.2712.

Sandved-Smith, L., C. Hesp, J. Mattout, K. Friston, A. Lutz, and M. J. D. Ramstead. 2021. "Towards a Computational Phenomenology of Mental Action: Modelling Meta-Awareness and Attentional Control with Deep Parametric Active Inference." *Neuroscience of Consciousness*: niab018. doi:10.1093/nc/niab018.

Scheffer, M., J. Bascompte, W. A. Brock, V. Brovkin, S. R. Carpenter, V. Dakos, H. Held, E. H. van Nes, M. Rietkerk, and G. Sugihara. 2009. "Early-Warning Signals for Critical Transitions." *Nature* 461: 53–59. doi:10.1038/nature08227.

Schooler, J. W., J. Smallwood, K. Christoff, T. C. Handy, E. D. Reichle, and M. A. Sayette. 2011. "Meta-Awareness, Perceptual Decoupling and the Wandering Mind." *Trends in Cognitive Sciences* 15(7): 319–326. doi:10.1016/j.tics.2011.05.006.

Smith, H. L. 1995. *Monotone Dynamical Systems: An Introduction to the Theory of Competitive and Cooperative Systems*. Mathematical Surveys and Monographs 41. Providence, RI: American Mathematical Society.

Suzuki, T. 2026. "The Dynamics of Entry into Attention: A Point Process of Candidate Openings toward Functional Non-Closure." Research Institute of Business Administration, Waseda University, Working Paper No. 2026-008. https://www.waseda.jp/fcom/riba/assets/uploads/2026/08/RIBA_WP2026-008.pdf.

van de Leemput, I. A., M. Wichers, A. O. J. Cramer, D. Borsboom, F. Tuerlinckx, P. Kuppens, E. H. van Nes, et al. 2014. "Critical Slowing Down as Early Warning for the Onset and Termination of Depression." *Proceedings of the National Academy of Sciences* 111(1): 87–92. doi:10.1073/pnas.1312114110.

Watanabe, T., and Y. Sasaki. 2015. "Perceptual Learning: Toward a Comprehensive Theory." *Annual Review of Psychology* 66: 197–221. doi:10.1146/annurev-psych-010814-015214.

Watkins, E. R., and S. Nolen-Hoeksema. 2014. "A Habit–Goal Framework of Depressive Rumination." *Journal of Abnormal Psychology* 123(1): 24–34. doi:10.1037/a0035540.

Wood, W., and D. Rünger. 2016. "Psychology of Habit." *Annual Review of Psychology* 67: 289–314. doi:10.1146/annurev-psych-122414-033417.